

High-resolution spectroscopic analysis of the pulsation frequencies and modes of three γ -Doradus stars: HD 139095, HD 48501 and HD 197541

G. J. Chappell
MSc by Research
University of York
Physics
October 2019

Abstract

Using the variability of light from pulsating stars to study the internal physics is a field called asteroseismology. γ -Doradus stars were the class of pulsators chosen, because of their unique pulsation mechanism. They are categorised as g-mode pulsators because the restoring force is gravity; this means the pulsations originate from deep inside the stellar interior, which provides us with important information about stellar structure. Using high-resolution spectroscopic data, the frequencies and modes from three γ -Doradus pulsating variable stars, HD 139095 and HD 48501 and HD 197541 have been determined. Long term observations have yielded 257 spectra for HD 139095, 165 spectra for HD 48501 and 309 spectra for HD 197541. The data were obtained from the 1.m McLellan telescope at The University of Canterbury Mount John Observatory using the High Efficiency and Resolution Canterbury University Large Echelle Spectrograph. The data were processed using a cross correlation technique that maximises the signal-to-noise ratio of the spectral line profiles. The non-radial pulsation modes of these profiles have been determined using a pixel-by-pixel Fourier parameter fit method. HD 139095 had five significant frequencies $f_1=1.22624 \pm 0.00001 \text{ d}^{-1}$, $f_2=0.59456 \pm 0.00002 \text{ d}^{-1}$, $f_3=1.38710 \pm 0.00002 \text{ d}^{-1}$, $f_4=1.13233 \pm 0.00001 \text{ d}^{-1}$ and $f_5=0.49500 \pm 0.00002 \text{ d}^{-1}$. Modes of (1,1), (2,-2), (3,0) and (2,-2) were identified for f_1 , f_2 , f_3 and f_4 respectively. HD 197541 had six frequencies of $f_1=0.71409 \pm 0.00001 \text{ d}^{-1}$, $f_2=1.01804 \pm 0.00002 \text{ d}^{-1}$, $f_3=0.82275 \pm 0.000007 \text{ d}^{-1}$, $f_4=0.76269 \pm 0.00002 \text{ d}^{-1}$, $f_5=1.11593 \pm 0.00002 \text{ d}^{-1}$ and $f_6=2.52637 \pm 0.00003 \text{ d}^{-1}$. Frequencies f_1 , f_2 , f_3 , f_4 and f_6 had the modes (3,-2), (2,-2), (3,-3), (3,-2) and (3,-1) respectively. HD 48501 had four frequencies $f_1=1.29042 \pm 0.00003 \text{ d}^{-1}$, $f_2=1.09386 \pm 0.00005 \text{ d}^{-1}$, $f_3=1.35816 \pm 0.0002 \text{ d}^{-1}$ and $f_4=1.23804 \pm 0.0002 \text{ d}^{-1}$. All the frequencies had modes of (2,-2), (2,-2), (2,-2) and (3,-3) respectively. It can be confidently stated that the target stars had full frequency and mode identification performed upon them, an important step to understanding these complex pulsation modes of γ -Doradus stars.

Contents

1 Acknowledgements	1
2 Declaration	1
3 Introduction	2
3.1 History of Pulsating stars	2
3.2 Radial and Non-radial pulsations	4
3.3 Driving Mechanism	6
3.4 Observational techniques	7
3.5 Rotational Effects	8
3.6 HD 197541	9
3.7 HD 139095	9
3.8 HD 48501	10
4 Methods	12
4.1 Acquisition of Data	12
4.2 Hercules Reduction Steps	13
4.3 4-Port reduction	14
4.4 Farns Preparation	16
4.5 FAMIAS	17
4.6 Error Calculations	18
5 HD 139095 Results	20

5.1	Cross-Correlation function	20
5.2	Frequency Identification	20
5.3	Fourier Parameter Fit and Mode Identification	23
5.4	Discussion HD 139095	24
6	HD 197541 Results	25
6.1	Cross-correlation function	25
6.2	Frequency Identification	26
6.3	Fourier Parameter Fit and Mode Identification	28
6.4	Discussion HD 197541	29
7	HD 48501 Results	30
7.1	Cross-correlation function	30
7.2	Frequency Identification	30
7.3	Fourier Parameter Fit and Mode Identification	32
7.4	Discussion HD 48501	33
8	Sources of error	34
9	Further discussion and conclusions	34
10	Appendix	36
10.1	HD 139095 phase and amplitude profiles	36
10.2	HD 197541 phase and amplitude profiles	37
10.3	HD 48501 phase and amplitude profiles	39

1 Acknowledgements

I would like to thank my supervisor Dr. Emily Brunsten of the University of York for her valuable support and guidance throughout this research; the University of York physics department for the facilities in which to conduct this research and everyone who helped obtain the valuable high resolution spectroscopic data at the UCMJO.

2 Declaration

I declare that this thesis is a presentation of original work and I am the sole author. This work has not previously been presented for an award at this, or any other, University. All sources are acknowledged as References.

3 Introduction

Stars are the life force of the Universe, they are the fundamental reason that life on Earth exists and so understanding them in as much detail as possible is one of the main goals of astrophysics and even science as a whole. Different information can be found by different methods, photometry can reveal their luminosity, effective temperature and even chemical composition by measuring the electromagnetic radiation. Spectroscopy, analysing a wavelength spectrum of light, along with other applications can be used to gain an insight into the interior structure of a star. Using spectroscopy to analyse the internal stellar structure of a star relies upon it to have intrinsic radial or non-radial pulsations. These are observed by a shift in the spectral lines because of the velocity variation as the parts of the star move towards and away from the observer. This is observed as a pulsation frequency and FAMIAS, which is a frequency and mode identification software, will then fit models to determine each frequency's mode. The type of star we will be analysing is the variable type, γ -Doradus (γ -Dors). The reason for this is because of their pulsations being driven by g - *modes*, that probe deeper into the interior than other pulsations.

This project will utilise advanced spectroscopic techniques to identify the frequencies and modes of pulsation in three γ -Doradus non-radially pulsating variable stars. These data are extremely useful and can be used to indicate the internal stellar structure of these stars. This field of astrophysics is called asteroseismology. Gaining as much data as possible to create more accurate models is essential in the progression of asteroseismology as a field.

3.1 History of Pulsating stars

Stars have been known to have a periodic change of magnitude since the first variable was identified in 1638, Omicron Ceti [1]. Commonly known as Mira, it was discovered by Johannes Holwarda and is a pulsating red giant with a variable period of around 11 months. The importance of this discovery was extraordinary sparking a significant observational effort to identify more of these variables and discover the reason for their pulsation. This gave birth to a new field of astrophysics called asteroseismology. Asteroseismology is the study of pulsations in stars; these pulsations are directly related to the internal characteristics of that star. Currently there are over 400,000 known variables all of which are classified depending on their pulsating characteristics [2]. Specific stellar pulsations are found at different points throughout the Hertzsprung-Russell (HR) diagram. It is therefore possible to construct instability strips of each pulsators position in the HR diagram.

The first star observed to show the pulsating characteristics of what is now known as a γ -Doradus variable was HD 27290 (a now confirmed γ -Dor). As a main sequence early F-type star, it showed periodic light variations of several hours which are too long to be attributed to p-mode pulsations as seen in δ -Scuti variables [3]. First discovered in 1963, it wasn't until over 30 years later that enough evidence of variables with similar pulsation patterns was found to confirm a new classification of pulsator. This classification is as follows: Variable stars with spectral type A7-F5; Luminosity class IV/V and with variations consistent with the model of high-order (n), low-degree (l), non-radial gravity-mode oscillations. From an observational point of view, γ -Doradus variables have pulsation periods between 0.4 and 3 days [4]. This class has a localised position on the Hertzsprung-Russell diagram, on or near the main sequence at the red edge of the classical instability strip (shown in figure 1), which indicates γ -Dors share a similar overall structure [5].

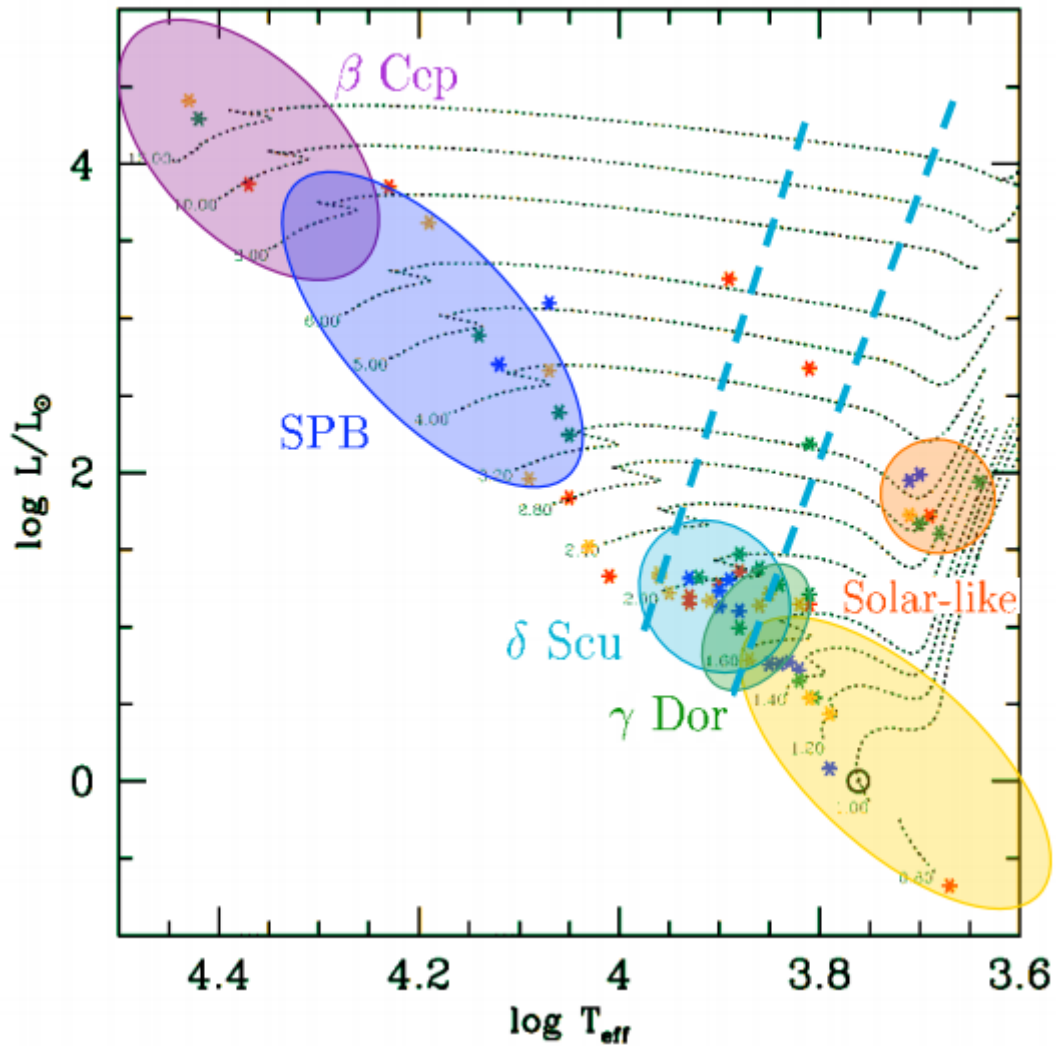


Figure 1: Hertzsprung-Russell diagram showing the overlap of δ -Scuti and γ -Doradus instability regions, the classical instability strip is indicated by the dashed lines. Slowly pulsating B-type stars are dark blue; β -Cepheids are purple; δ -Scutis are light blue; γ -Dors are green; Solar like stars are yellow and the red stars represent Semi-regular pulsators. [6]

The asteroseismology of γ -Dors is currently going through an exciting period thanks to recent efforts to observe exoplanets. Several space missions have been launched that are designed to use photometry to detect the variability of stars caused by a planet passing through the line of sight. Fortunately for asteroseismologists, these data will also detect a significant amount of pulsating stars. The CoRoT space mission, which stands for Convection, Rotation and Planetary Transits, is another dedicated exoplanet detection program. Launched in 2005 it observed over 180 000 stars during its seven-year mission duration. It had two Charge-coupled devices that observe through an afocal telescope with a 27cm aperture. Observations consisted of "long runs" between two and five months in duration that were devoted to exoplanet detection and asteroseismology studies, and "short runs", between one and six weeks that were used for additional science programs [7]. The NASA *Kepler* mission was launched in 2009 and collected wide-field photometric observations in the constellations of Cygnus and Lyra. After a hugely successful mission providing light curves of tens of thousands of stars, and massively contributing to the identification of many pulsating stars, the loss of two reaction wheels ended the mission. NASA re-purposed *Kepler* for it's second mission (K2), in 2014. This missions main objectives were to

advancing fields in exoplanet research, star formation, supernovae and asteroseismology by observing around forty thousand targets [8].

The Transiting Exoplanet Survey Satellite (TESS) is a NASA satellite that is performing a near all-sky survey for planets that transit near bright stars. Launched in April 2018, TESS employs four identical cameras for a combined field of view of $24^\circ \times 96^\circ$. It will observe from a thermally stable, low-radiation high-Earth orbit and, over its two year mission, observe nearly the whole sky. Of the 2×10^5 pre-selected targets all three of the γ -Dor stars in this project are expected to be observed. It is observing in 26 separate sectors of sky each lasting for 27.4 days. This is enough time for TESS' advanced photometric detectors, capturing images every two seconds when in short cadence mode, to observe the pulsations of γ -Dors [9].

Recent studies have also focused on γ -Doradus and δ -Scuti hybrid variables. δ -Scuti stars have a spectral type of A0/FV and are found to have effective temperatures between 7000K and 8500K. The instability strips of γ -Doradus and δ -Scuti Stars partially overlap in the Hertzsprung-Russell diagram suggesting the existence of variables showing both pulsation types. A large sample of *Kepler* and CoRoT stars indicated that this hybrid behaviour might be common in A-F type stars and further studies by Uytterhoeven in 2011 revealed that 36% of a sample of over 750 γ -Dor/ δ -Scuti candidates are hybrid [10]. A more recent study by Bradley in 2015 with a larger sample strongly suggest the occurrence may be even more common [11]. The possibility of having δ -Scuti/ γ -Doradus hybrid variables makes it difficult to accurately categorise these stars affirming the importance of improving spectroscopic observation techniques.

Currently the number of mode identifications fully complete for γ -Doradus stars is extremely lacking. Of all the bona fide γ -Doradus variables identified to date only a small percentage have had full geometric mode identifications scientifically published. For example, HD 12901 was analysed in 2018 to determine five frequencies, $f_1 = 1.3959 \text{ d}^{-1}$, $f_2 = 1.1863 \text{ d}^{-1}$, $f_3 = 1.6812 \text{ d}^{-1}$, $f_4 = 1.2157 \text{ d}^{-1}$ and $f_5 = 1.5596 \text{ d}^{-1}$ all with modes of $(l,m)=(1,1)$ [12]. This makes it an excellent candidate to test models of non-radially pulsating γ -Doradus stars. A total of 591 spectra was obtained during that project, outlining the significant amount of time and effort needed to perform accurate frequency and mode identification. Spectroscopic verification of known γ -Doradus variables, identified with photometry, is also generally lacking where in some cases the two observation results categorically disagree. HD 12901 was observed just using photometry in 2002 and only three frequencies were determined $f_{p1} = 1.21562 \text{ d}^{-1}$, $f_{p2} = 1.39594 \text{ d}^{-1}$ and $f_{p3} = 2.18637 \text{ d}^{-1}$ [13]. f_{p1} and f_{p2} are observed in both projects, however even with the vast amount of spectra obtained in the spectroscopic observations f_{p3} isn't identified. It does appear to be a one-day alias of f_2 and is therefore not intrinsic to the star. This problem of photometric observations claiming aliases, harmonics and combinations as intrinsic frequencies to the star is an issue that needs to be resolved. More spectroscopic research has to be completed with the aim to eradicate these discrepancies.

3.2 Radial and Non-radial pulsations

There are two ways in which stars pulsate: radially and non-radially. Radial pulsations are completely symmetrical; the entire surface expands and contracts equally. Non-radial pulsations are not spherically symmetric and therefore have nodal and anti-nodal lines on the surface. Spherically-symmetric radial modes can be classified by a singular number, radial order (n) this describes the number of spherically symmetric nodal shells that are present within the star. Non-radial pulsations need to be classified by three numbers: n , radial order; l , degree and m , azimuthal order. Degree is the total number of nodes present on the surface of the star and azimuthal order (m) is the number of these nodes which intersect with the poles of the rotation axis. Azimuthal order, m must lie between $[-l \text{ \& } l]$.

The deviation from spherical symmetry in non-radial pulsation modes means, mathematically, we obtain a large number of possible oscillation modes using spherical harmonics:

$$Y_l^m(\theta, \phi) = N_l^m P_l^{|m|}(\cos\theta) e^{im\phi}, \quad (1)$$

where θ is the angle from the polar axis, ϕ is the longitude, $P_l^{|m|}$ is the associated Legendre polynomial, N_l^m is a normalisation constant and l and m are spherical degree and azimuthal order. Using:

$$P_l^m(x) = (-1)^m (1-x^2)^{m/2} \frac{d^m}{dx^m} P_l(x), \quad (2)$$

It is possible to obtain the following solutions:

$$P_0^0(\cos\theta) = 1, \quad (3)$$

$$P_1^0(\cos\theta) = \cos\theta, \quad (4)$$

$$P_1^1(\cos\theta) = -\sin\theta, \quad (5)$$

$$P_2^0(\cos\theta) = \frac{1}{2}(3\cos^2\theta - 1), \quad (6)$$

$$P_2^1(\cos\theta) = -3\cos\theta\sin\theta, \quad (7)$$

$$P_2^2(\cos\theta) = 3\sin^2\theta, \quad (8)$$

and so on.

Pulsation modes with $m \neq 0$ are travelling waves and can be defined by applying the equation for spherical harmonics, they can run with or against the rotation of the star.

The non-radial pulsations divide the stellar surface in regions of different velocity and temperatures. The velocity fields therefore give rise to local Doppler shifts, and because of the stars rotation, their variations are Doppler mapped to the absorption-line profiles, creating a moving pattern of peaks and troughs. An example is given in figure 2. A star showing these pulsations typically shows more than one of these modes of oscillation, all of which are described by the equations 3 through 8. There are many factors that affect a given mode's oscillation, the most important of which is the driving mechanism responsible for the pulsation.

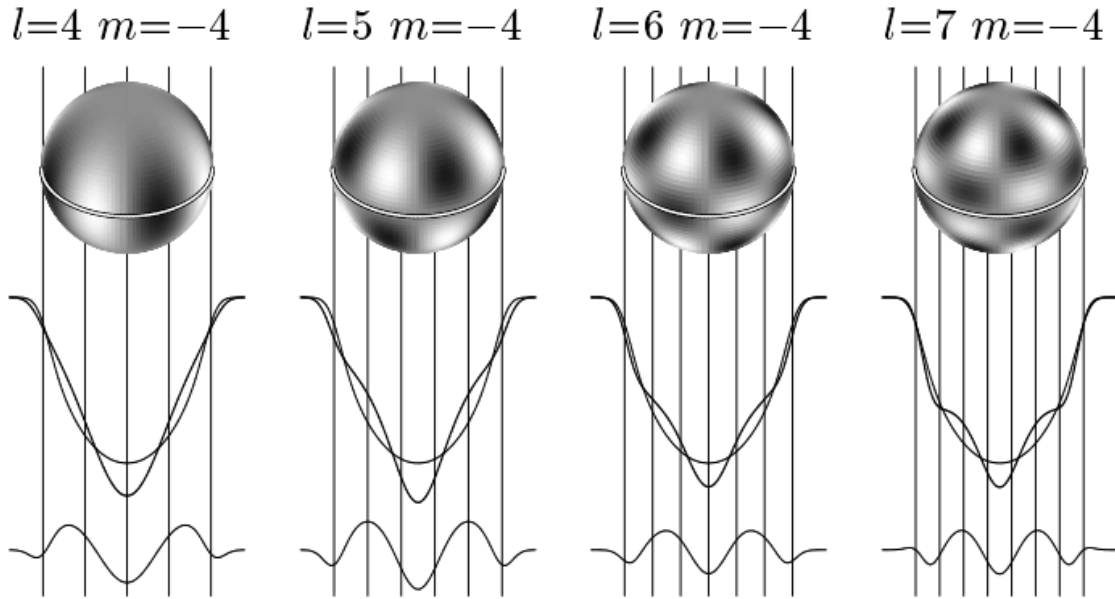


Figure 2: Line profile variations in direct comparison with the mapped Doppler shift. The top section shows a spherical model of a pulsating star where the shaded regions show the velocity shifts. The middle section directly shows the line profile variation corresponding to the velocity shifts, superposed onto a non pulsating line profile. The bottom row is a representation of the difference between the line profiles of the pulsating and non pulsating case [14]

3.3 Driving Mechanism

Stars are in hydrostatic equilibrium: the gravitational pull of the star is equally balanced by gas pressure. If an external force were to compress the outward region of the star, the inward moving areas are heated and that resultant heat loss damps the motion. Therefore a pulsating star must have a method of self-exciting, this requires a driving mechanism.

The $\kappa - \gamma$ mechanism; in the stellar interior there are layers where the opacity κ increases and/or the third adiabatic component (the magnetic flux enclosed in the layer) decreases causing flux from the inner layers to be temporally stored at the opacity boundary. These layers occur because of ionisation of certain chemical components in that layer. This accumulated energy builds up pressure and causes the layer to readjust its equilibrium state by expanding, in turn making the star expand past its equilibrium radius. The trapped energy is released and the star recedes back to its initial state and the whole cycle repeats. This mechanism describes a large majority of the current classes of pulsating variables including δ -scuti stars [14].

γ -Dors pulsate via a different mechanism, although similar to the $\kappa - \gamma$ mechanism, the key to this driving mechanism is the existence of a deep convective envelope. This convective zone has temperatures of 170,000 to 450,000 Kelvin and at these temperatures the local convective timescale is equal or longer than the pulsation period. An adiabatic approximation can therefore be used, for which we assume entropy remains constant. The comparatively long convective timescale means the convection cannot adapt quickly enough during the pulsation to transfer the radiation emerging from the core, resulting in it being blocked, causing the driving mechanism [15]. One of the main advantages of analysing γ -Dors as opposed to the other variables mentioned, is this difference in pulsating mechanisms. The convective blocking originates from deeper in the stellar interior; revealing information about the core of the star that is inaccessible by other pulsating mechanisms.

There are two major restoring forces for these oscillation mechanisms that try and return the star to its equilibrium position; pressure and gravity. Radial pulsations are always restored by pressure, p-modes. As the star symmetrically compresses in a radial pulsation, the gravitational force in the star increases and this would cause the oscillation to accelerate not restore, so it is determined that pressure must always be the restoring force. Non-radial pulsations can not only have p-modes but g-modes where gravity restores the motion through buoyancy. The two sets of modes therefore differ in their direction of motion, p-modes are radial and g-modes are transverse. γ -Doradus stars mainly pulsate through g-modes caused by the previously mentioned convective blocking mechanism. Other types of modes exist such as: g^- -modes, convectively excited g-modes and strange modes that occur in environments of a highly non-adiabatic environment. These modes will not be considered in this project further because to date there is little practical importance of them in the seismic sounding of stars [14].

The most important parameter of determining the evolution of main-sequence stars is the mass of the core. Stellar core convection can mix material in the radiative layer into the core significantly altering the mass. This phenomenon is called convective core overshooting and there is not much understanding of it even though it can have huge impacts on stellar life-time [16]. Overshooting also decreases the gradient in the mean molecular weight at the edge of the core, this means the frequency of the lowest order g-mode measures the convective core size, an invaluable quantity for astrophysicists. Using spectroscopy and photometry to observe these g-modes is the most effective way to get a glimpse into the deep stellar interior.

3.4 Observational techniques

Two major observational techniques are widely used to study variable stars: Photometry and spectroscopy. Photometry uses a photometric detector such as a Charge Coupled Device (CCD) to quantify the flux of electromagnetic radiation detected from the the target star. Comparing with a fixed star (or using a different calibration technique) the change in incident flux with time can be measured. Using this information, the target star's variation in absolute magnitude and luminosity can be determined. There is currently a large amount of photometric observational activity surrounding pulsating variables. Data from MOST, CoRoT, HIPPARCOS and *Kepler* are all being used in analysis of γ -Doradus stars. The HIPPARCOS mission collected observations for 118,000 stars. Over its 3.3 year mission it gained information about position, magnitude, colour, spectral and variability types, radial velocity and multiplicity [17]. In 1998 a study using these data published the discovery of fourteen new γ -Doradus stars, all having their periods determined. five stars had their $v \sin i$ values determined including HD 40745 with a moderate $v \sin i$ of 33 km s^{-1} [18], which makes it an ideal candidate for full spectroscopic mode identification. To study stellar pulsation using photometry it is necessary to use integration time shorter than the pulsation period to ensure many data points are collected at different sections of the pulsation cycle. Therefore integration times for asteroseismology are often selected to be around 10 s. This allows for fast data acquisition. The rapid speed of data acquisition is the reason photometry is preferred for large survey missions such as the missions stated above. Using single-colour photometry alone, only the spherical degree of a given pulsation mode can be identified. In order to determine the azimuthal order spectroscopy must be involved. Photometric observations are therefore best used in initially finding candidates for further spectroscopic analysis.

The use of spectroscopy to determine modes and frequencies of a pulsating star relies upon the radial velocity variations on the stellar surface. As these sections move inwards and outwards the spectral line profiles are Doppler shifted. This shift can be measured and described as a function of time against phase and amplitude. From this, spherical degree, l and azimuthal order, m can be determined and used to describe the mode of pulsation. High-resolution spectroscopy is required to determine the variations in the line profile, this is because the small scale of the variations are hard to identify if the spectra are not of a high resolution. In stark contrast to the average 10 – sec integration time used for

photometry, spectroscopy requires a much longer exposure time, decreasing the rate of acquisition. This is one reason why spectroscopic observations are confined to the ground. Another being the nature of different oscillations. Some but not all modes can be excited at different times, it is therefore important to have continuous observations for extended periods of time to accurately observe all possible pulsation modes.

Spectroscopic data has been used previously to identify frequencies and modes in γ -Doradus stars. An example of this was done in a project on HD 189631 and HD 40745. The stars had a full frequency and mode identification performed using FAMIAS, a frequency and mode identification software. A Fourier analysis method was used to obtain the frequencies: $f_1=1.167\text{d}^{-1}$, $f_2=1.42\text{d}^{-1}$, $f_3=0.07\text{d}^{-1}$ and $f_4=1.82\text{d}^{-1}$ for HD 189631 and $f_1=0.74\text{d}^{-1}$ and $f_2=1.09\text{d}^{-1}$ for HD 40745. HD 189631 had four modes identified at $(l = 1, m = 1)$, $(3, -2)$, $(2, -2)$ and $(4, 1)$ and HD 40745 had two $(l = 2, m = -1)$ and $(3, -3)$. It was the first full spectroscopic analysis of the two stars and proved to be a successful endeavour [19].

It is extremely important to obtain time-series data with a high Signal-To-Noise ratio (SNR) because the analysis and mode identification can be hugely limited by the presence of noise and gaps in the data. When determining frequencies, only those with a $SNR \geq 4$ can be considered, if the noise is too large, important frequencies can be lost. Gaps in the data occur when there is an absence of enough data points throughout the whole of a stars pulsation cycle, this can affect the accuracy of the determined fit and any conclusions drawn from it. The techniques utilised to maximise the SNR, like the cross-correlation technique, are detailed in the method section.

Spectroscopy can also indirectly be used to identify the age of pulsating stars. Rotational velocity, $v \sin i$ is another parameter that is identifiable using spectroscopic data and studies of hundreds of stars in a range of spectral types show a trend, within the main sequence, between rotation rate and age. Early-type stars O, B and A have rotational velocities above 200 km s^{-1} and that from spectral type F, there is a decline from 100 km s^{-1} to 10 km s^{-1} at G. Since it can be stated stellar rotation declines over time it is possible to use the determined rotational velocity to determine the age. This method is called "gyrochronology" and although this method is reliant upon the rotation of stars, this rotation can have a detrimental affect on other analytical processes [20].

3.5 Rotational Effects

A pulsating star's rotation affects its oscillation frequencies because of the distortion caused by the centrifugal force. This effect has a higher impact upon p -modes with small inertia and a higher sensitivity to the outer layers of the star but the effects on g -modes must also be considered. Rotation rates have another adverse affect specific to γ -Dors: The relatively fast rotational period is sometimes similar to that of the pulsation period (around one day), producing anomalous periodicities in the phase diagram which can interfere and cover the pulsation modes. This rotation can, however, be extremely useful in γ -Dors; for it to be possible to determine variations in the spectral line profile the position of the profile must accurately determined. A fast rotation rate aids this by broadening the spectral line profile, making its position easier to determine. The broadening must be significantly larger than the local line profile at a singular point on the stellar surface, then fluctuation at that point will result in a measurable bump in the profile. This bump moves across the the profile as the star rotates. If the time series is inverted the result is a map of the stellar surface.

There has been recent work done on identifying a new type of mode directly related to rotation, Rossby modes (r -modes). These modes unlike, p -modes and g -modes, use inertia as their restoring force. They are made visible by the compression, caused by the Coriolis force, increasing the tempera-

ture at points on the stellar surface. These waves propagate in the direction of rotation and would make it possible to measure the inclination of rotation in the future by modelling these pulsations found in the spectra. This opens up the ability to be able to study the inner physics of main-sequence stars with differential rotation when coupled with g -modes. This will significantly affect γ -Dors because they are one of the main candidate stars for observing r -modes, thanks to their moderate-to-high rotation rates [21]. This outlines the positives and negatives effects that appear from a star's rotation rate. The criteria for an ideal target star therefore must have a moderate-to-high rotation rate.

3.6 HD 197541

HD 197541 is a F0IV/V star located in the constellation Microscopium. An interesting aspect of this star is the fact that it is part of a double star system as shown in the image in figure 3. It has an apparent magnitude of 6.84 while its companion star has an apparent magnitude of 11.0 and has a separation of 9.78 arc seconds [22]. Fortunately its relatively large separation and dim companion star suggest that it will have a negligible affect on the results obtained in this project.

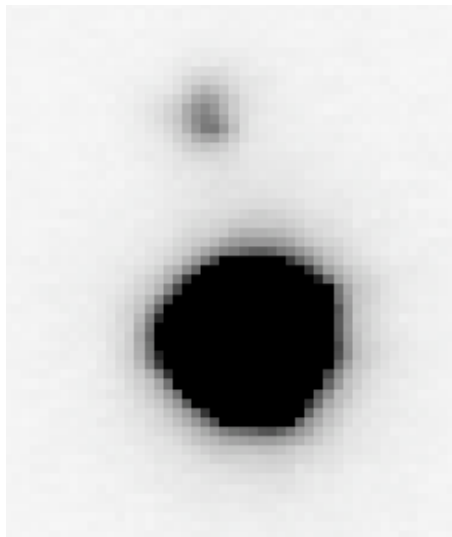


Figure 3: Image of an over exposed HD 197541 and dim companion star, taken using the HERCULES guide camera. [23]

Identified as candidate γ -Doradus star in 1999 using Hipparcos photometry [24], It was discovered to be multi-periodic with two periods identified as 1.400 and 1.093 days. With a $v \sin i$ value of 29 km s^{-1} it's classified as a moderate rotator [25]. These are characteristics typical of a γ -Dor. This is the limit of the previous published work on HD 197541's periodicity. There is clearly a lot more analysis that can be performed upon it, especially as TESS performed a photometric observation commencing on the 25th of July 2018. It had exposure times of 120s for the full 27.4 days [26]. The data was released on the 6th of December 2018 and will be able to support future spectroscopic analysis of this star.

3.7 HD 139095

HD 139095 is an A9/F0 V spectral type star found in the constellation Lupus with a reasonably dim apparent magnitude of 7.91 [27]. It has been confirmed as a bona fide γ -Doradus using HIPPARCOS

photometric data which uncovered a single period of 0.634 days [24], it was initially thought to belong to δ -Scuti type variables, however, a later study suggested that the light curves were multi-periodic with no evidence of δ -Scuti variability to a limit of 1.1 mmag [28]. The known observational parameters of this star are outlined in table 1.

V (mag)	$B - V$ (mag)	M_V (mag)	$L(L_\odot)$	$R(R_\odot)$	Period(d)
7.91	0.366	2.62	7.0	1.9	0.634

Table 1: Table displaying the known observational parameters for HD 139095, [28].

HD 139095 was selected in an eleven γ -Dor star sample for photometry and spectroscopy analysis [27]. Although confirming the multi-periodic variability there was not enough spectroscopic data to identify the other periods (other than 0.634 days) or complete any mode identification on the one known frequency. Its spectral type, period and $v \sin i$ of 65.3 km s^{-1} [29] are typically expected from a γ -Dor. HD 139095 was also selected for spectroscopic analysis in 2008 [30]. Observations lasted three weeks and collected 57 spectra. Although frequency identification was performed obtaining $f_1 = 2.353 \text{ d}^{-1}$, $f_2 = 9.560 \text{ d}^{-1}$, $f_3 = 8.638 \text{ d}^{-1}$ and $f_4 = 10.14 \text{ d}^{-1}$ [30], the frequencies seem to be too large, suggesting that due to the short time-base of the observations noise would have been a large issue. The result appears to be the identification of harmonics and alias frequencies that aren't intrinsic to the star. Again, due to the three week observation period and limited spectra it was stated that the mode identification suffered from poor fits with only f_4 having a mode of $(7 \pm 1, 5 \pm 2)$ with the authors admission that HD 139095 required more spectra and better quality data for precise analysis. TESS is planned to observe HD 139095 during the second half of its two-year mission. This data will be used in the future in unison with spectroscopic data to analyse this star.

3.8 HD 48501

HD 48501, found in the constellation of Canis Major it has an apparent magnitude of 6.26 and is identified as a F2V type star [31]. It has had the most extensive photometric and spectroscopic analysis compared to the other target stars. It was initially identified as a γ -Doradus in 2000 with a dominant period of 0.7750 days [31]. This was identified using the photometric data from the Geneva catalogue [31], a union of more than 200 scientific programs. The phase diagram used to identify the period is shown in figure 4. It has an amplitude of 12.8 mmag and was stated to be clearly multi-periodic. A second period was identified as over 10 days but this was discounted as an alias caused by the measured $v \sin i$ of 40 km s^{-1} .

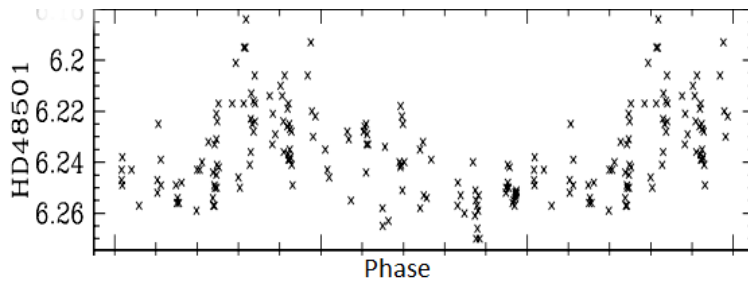


Figure 4: Phase diagram of the V-magnitude for HD 48501 used to identified the period [31].

A long-term multi-colour photometry and high-resolution spectroscopy of HD 48501 was published in 2004 [32]. Again using the Geneva data, this time it was analysed in parallel with spectroscopic data. The data consisted of 184 photometric measurements obtained from a 0.7 m telescope stretching over 20 years. The spectroscopic data was gathered with CORALIE Echelle spectrograph attached to a 1.2m telescope, 34 high-resolution spectra was obtained with a time base of around three years. Three frequencies were identified to be $f_1 = 1.09408 \text{ d}^{-1}$, $f_2 = 1.29054 \text{ d}^{-1}$, $f_3 = 1.9924 \text{ d}^{-1}$. A time-series

cross-correlation function was obtained using the spectroscopy, figure 5. A more accurate $\nu\sin i$ was also measured to be $29 \pm 2 \text{ km s}^{-1}$ using the cross-correlation function. Modes were identified for the three frequencies as all $l = 1$. This mode determination was completed over 15 years ago and hence these results will need to be validated during this project, with a much larger data set. In January 2019, TESS captured HD 48501 on two CCDs, with exposure times of 120s and 1425.6s. The exposure time of 120s is used to obtain data that will be useful for asteroseismology because the shorter cadence is more able to accurately sample the light curve of the pulsation. These data were released on the 11th of March 2019, and will be used in tandem with high-resolution spectroscopy in future analysis of this star.

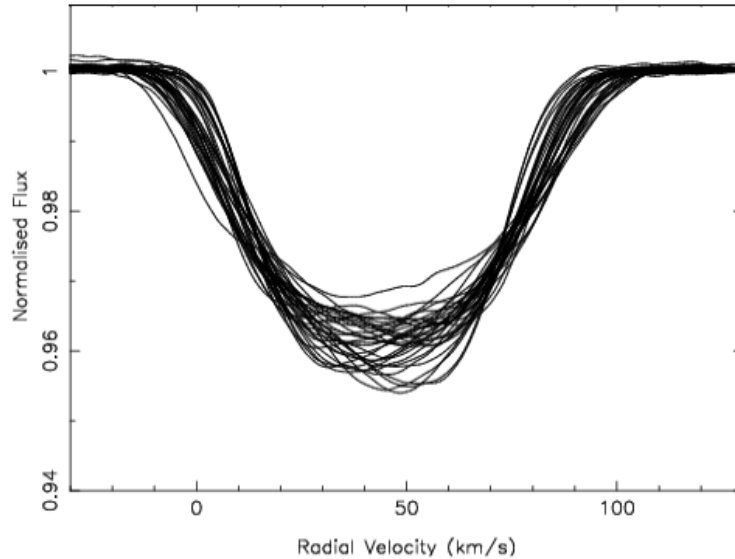


Figure 5: Cross-correlation function of HD 48501 from the CORALIE Spectrograph [32].

These stars were chosen for frequency and mode identification because they are all candidate or confirmed γ -Dors showing multi-periodicity. They all have moderate $\nu\sin i$ shown in table 2, a criteria for accurate spectroscopic analysis. The rotation rate can potentially be used for Rossby mode identification in the future as discussed previously. This used in tandem with the g-mode analysis of γ -Dors will allow for accurate comparisons of the affects of rotation rate on the stellar interior. The selection process was to choose γ -Dors that have had periods confirmed by photometry but lack mode identification due to limited spectroscopic analysis. This has the importance to compare spectroscopic and photometric techniques which is one of the key aims. Another aim to be completed in this project is the full mode identification of the target stars to derive progress towards important information regarding the stellar interior.

HD 48501	HD 197541	HD 139095
29 km s^{-1} [33]	29 km s^{-1} [23]	65.3 km s^{-1} [29]

Table 2: Table showing the literature values for $\nu\sin i$ of the target stars.

4 Methods

4.1 Acquisition of Data

Spectroscopic data has been collected over a period of 10 years between October 2007 - December 2017 as part of the MUSICIAN project [34]. All the data are obtained using the High Efficiency and Resolution Canterbury University Large Echelle Spectrograph (HERCULES), with the 1-meter McLellan telescope at the University Canterbury Mount John Observatory (UCMJO)[35]. UCMJO is situated at an elevation of 1029 meters, at 170°, 27.9', East; 43°, 59.2', South. The spectrograph is a fibre-fed instrument that has been designed to capture the entire wavelength range 380-880 nm in a single exposure and to do so while providing stability and reproducibility of the spectra. The entire spectrograph is housed in a large vacuum tank and maintained at a constant pressure of approximately 400 pascals. This ensures that changes in air pressure and temperature have a minimal effect on the stability of the spectrograph [35]. The spectrograph's Charge-Coupled Device (CCD) detector was upgraded in 2007 to a Fairchild 486 model, housing 4096 by 4096 pixels of size 15 micrometers. The CCD is chilled to a temperature of around 173K to reduce the effects of internal noise.

There were three types of data obtained: science observations, thorium-argon images and flat-field images. Thorium-argon data is collected in order to accurately perform a wavelength calibration. This is an extremely important step because without this, regardless of how advanced the Echelle spectrograph is, a precise wavelength calibration is still required to accurately determine the velocity shifts in the spectra. It is standard practice to use a thorium-argon lamp since Meggers in 1957 first suggested that thorium transactions might act as reliable wavelength standards [36]. Thorium-argon observations were taken during each hour every observation night, this is to account for small fluctuations in pressure and temperature to make the calibrations as accurate as possible.

Flat-fields are another extremely important aspect of the image calibration process. A flat-field is created by uniformly illuminating the CCD, it is used to extract the spectral orders and to eliminate imperfections in the optics and variations in the pixel-to-pixel sensitivity. The most accurate method of creating a flat-field and the one used in these observations was the use of a white tungsten lamp. These images were taken at the end or beginning of the observation night. Flat-fields are taken at exposures of around 1 second where thorium-argon images are slightly longer. An example of both of these calibration images is shown below in figure 6. The observational images are reduced in batches of one month and so the flats of that month must be summed together to create a summed flat that is used to remove all the imperfections that occurred during that period.

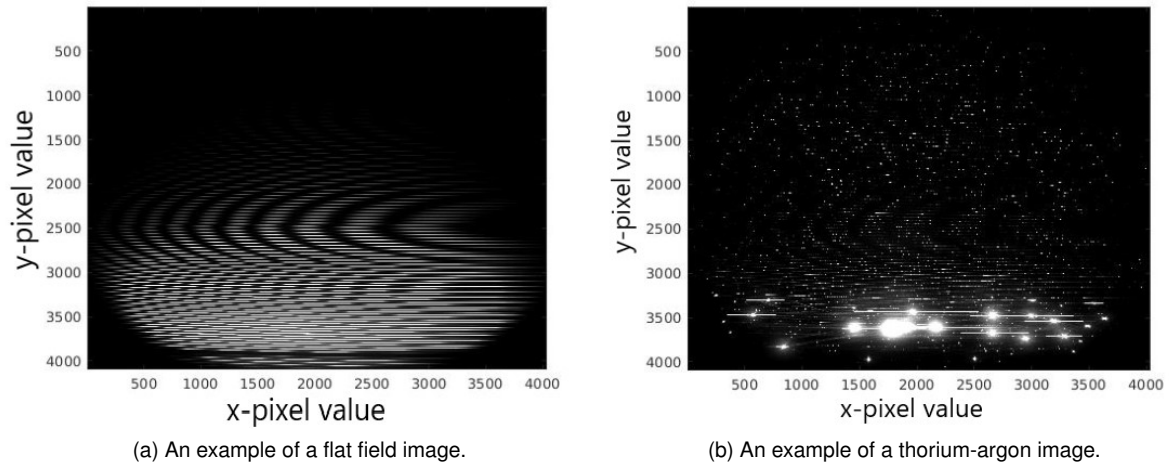


Figure 6: An example of a thorium-argon calibration image and a flat field white light image used in the data reduction process. The flat field shows the lines of the spectral orders more clearly than the thorium-argon image. The thorium-argon spectral lines can be seen traced along each spectral order with the orders at the bottom appearing to be over exposed.

There are a number of requirements for the spectroscopic data: Time series are fully reduced and normalised, including barycentric time and velocity correction; Dispersion is better than 40,000 and signal-to-noise ratio higher than 200. The standard exposure time of 20 minutes was used for the majority of the observations. During the acquisition period a total of 165 usable spectra was obtained for target star HD 48501, after removing anomalous and corrupted data. HD 139095 and HD 197541 had 257 and 309 spectra respectively. It is necessary to obtain hundreds of spectra for each target star because a different selection of modes can be excited at different points in the pulsation cycle. A full mode identification is only possible if a large number of spectra are obtained. γ -Dors pulsate in periods in the magnitude of one day, therefore an issue arises if observations are taken at the same time every night and so many spectra need to be acquired to get a full phase plot. The observational time baseline of the observations is given in table 3. The values, given in Julian date form, are used in the error calculations.

	HD 139095	HD 197541	HD 48501
Observation start date (BJD)	54876.1909	54411.9141	56229.1358
Observation end date (BJD)	56342.1983	57966.1725	58010.1817
Time baseline (BJD)	1466.0074	3554.2584	1781.0459
Number of observations	257	309	165

Table 3: Table displaying the observational time frame. Observational dates are given in Julian date form - 2400000 d

4.2 Hercules Reduction Steps

The the data preparation for the Fourier analysis was done in a Matlab pipeline, written by Dr.Duncan Wright and Dr.Emily Brunsten specifically for the spectroscopic data obtained by the HERCULES telescope [37]. As part of this project the reduction code was extended to be able to reduce the images taken with the 4-Port setting on the CCD. The code makes use of the headers inside the FITS file which

contain the observational data. These headers contain details about the file including the target star. This is how the script can quickly sort through the vast amount of data and select the relevant observations. Once the location of the specific star's spectrum file is obtained, the script then reduces the data, it is important to note that the script works best when reducing the data in sections, usually monthly instead of all at once.

The first step is flat-field calibration for the reasons explained previously. The relevant flat-field images are summed together and an automatic comparison is made that makes sure all the individual files have no significant differences. It is good practice to cut the first 1000 rows of the 4096 by 4096 pixel chip, this is because the blue end of the chip is too noisy to perform any useful analysis on. The result is a summed flat field image that is used throughout the rest of the reduction. The program traces the thorium-argon orders along the flat-fields defined axes and this will then be used to trace the stellar orders along.

The wavelength calibration is performed using the thorium-argon files, these are checked for any significant differences between each other. Images that may result in a poor wavelength calibration are removed. The lines in the images are identified using a pre-calibrated matrix. A new one of these matrices may need to be created if the vacuum tank housing the spectrograph is opened because this would cause temperature and pressure fluctuations. If not enough arc lines are identified it is up to the user's discretion whether or not the image should be used for the wavelength calibration. Ideally there would be over 1000 lines found but anything over 800 is acceptable. If there are no changes to the data files then this calibration can be re-used and is therefore saved for the next reduction to be processed. Using the locations of the spectral lines, a full set of wavelength calibrated axes is obtained.

The next section of the script processed all stellar images. The spectral orders of each calibrated image are extracted. After this a cosmic ray removal occurs to reject extraneous spectral features not originating from the target star. The intensity data along each order are then stored as arrays. The wavelength axes are corrected because of the systematic velocity shift of the star. This is inputted from values found in the literature shown in table 2. Other corrections are also applied to the data, such as the barycentric correction. When the light from the target star is observed, the Earth orbits the Sun and rotates around its axis. We have to therefore extract these movements from the radial velocity from the measured star. So we correct the observed radial velocity for the motion of the observer in the direction of the observation. This naturally depends on the position of the Earth and is time-dependent [38].

To date there is no automatic way to complete an accurate continuum fit. Instead this has to be done manually, by comparing the observed mean spectrum with a synthetic spectrum compiled by the program Synspec [39]. Synspec is a package written in FORTRAN for modelling stellar atmospheres and for stellar spectroscopic diagnostics, it generates a spectrum from known values of stellar parameters of rotational velocity, effective temperature and surface gravity. A smooth function is generated that each stellar spectrum is divided by, this normalises the mean stellar spectrum to match it as closely as possible to the synthetic data. The orders are finally merged to produce the wavelength calibrated and normalised stellar spectra which are ready for the line profile analysis.

4.3 4-Port reduction

To achieve an accurate wavelength calibration at least 800 thorium-argon lines need to be identified. For approximately two years worth of data only around 400-500 lines were being achieved. This issue had been discovered during previous reductions however the cause and solution of the problem were never determined. This was deemed not acceptable and an inquiry began to attain why such a large amount of data was unusable. After a large amount of analysis of the unusable data and comparing it

to the data that was processing correctly, it was found a possible answer lay in the headers of the FITS files. In a section that keeps a log of the technical set up of the CCD there was a difference noted by the Port Output column, for the good data a value of 1 was shown and for the unprocessed data a value of 4. The port value corresponds to the number of readout ports that the charged pixels can empty into. The benefits of having more readout ports is a reduced readout time and therefore a faster CCD re-set time, this increases the possibility to capture more images per session. There are other methods to do this however they sometimes affect the quality of the image, for example pixel binning which collects the pixels charge in groups before the readout, this is at the cost of resolution. The 4-ports allows the user to get faster readout times with minimal pixel binning so it is important that the reduction code is able to accommodate the data.

To achieve this, it was essential to understand the reason the script was rejecting so many arc lines. To see exactly what was different in the CCD, a cross chip plot of intensity against pixel number for both 4-port and 1-port was created. Shown in figure 7 below, there is a step half way through the chip. This is because each section of the 4-port chip has a different zero value. it was inferred from this that around half of the arc lines would be on each half of the chip creating a separation that results in half of the lines being wrongfully discarded.

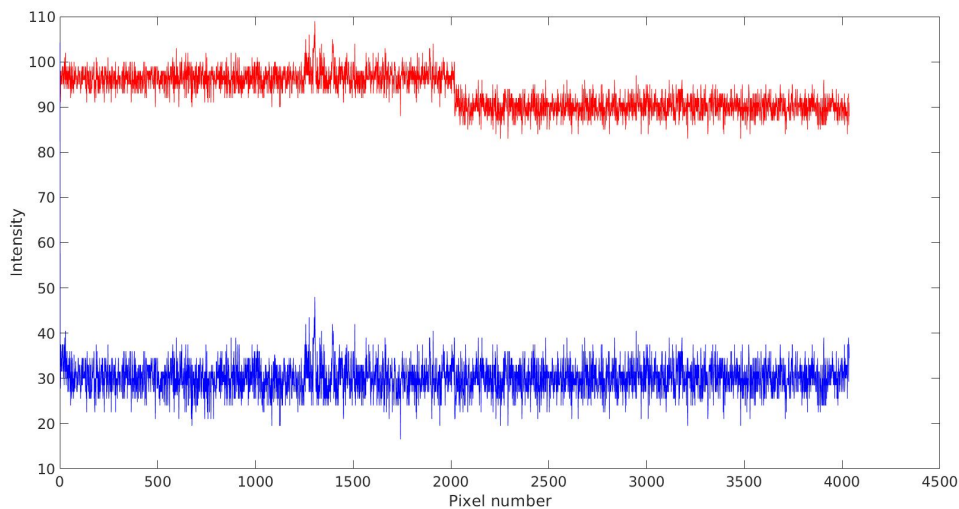


Figure 7: An example of the step in the 4-port flat field (red) and a 1-port flat field (blue). The difference in intensity is due to a longer exposure time used on the 4-port flat field image.

The decision to accept or reject lines occurs in the "processing all Thars" section of the script. It was decided that the two halves of the chip will be processed separately when producing the thorium-argon calibration and also the stellar files later on. The two halves are then combined at the end of the reduction before the FAMIAS preparation. This has been written in the script so that it automatically defines the 4-port files separately making the processing just as simple as the 1-port files. The reason the chip was split and processed separately, instead of adjusting the offset in one half of the chip, was because the exact offset value varied in each image. This would have made accurate automatic reduction of the data difficult. This solution, that was developed and coded explicitly as part of this project adds another dynamic to the results section, it is now possible to make a comparison between the two CCD port settings and flag any differences. The target star that is affected by the 4-port files is HD 48501 with 35 spectra having been obtained with the 4-port setting. This equates to 21% of the total spectra used in this project. It was not only important to resolve this issue because of HD 48501 but also for the future projects that will use the same Matlab reduction pipeline.

4.4 Farnas Preparation

An important section of the preparation for the line-profile analysis is the removal of unusable regions in the spectra. This is done by a manual inspection of the full spectra. Wavelength regions such as telluric and hydrogen Balmer are removed. Telluric regions are absorption lines caused by the Earth's atmosphere and so are mainly made of H_2O and O_2 . These regions become very noisy and it is hard to define particular spectral lines [40]. Hydrogen Balmer absorption lines $H\alpha$, $H\beta$ and $H\gamma$ regions are also unsuitable for analysis because they disguise the Doppler shifts because the lines are highly blended. The removed regions still need to be manually inspected and sometimes adjusted because of the spectral broadening that can occur, an example of the spectra removal process is shown in figure 8.

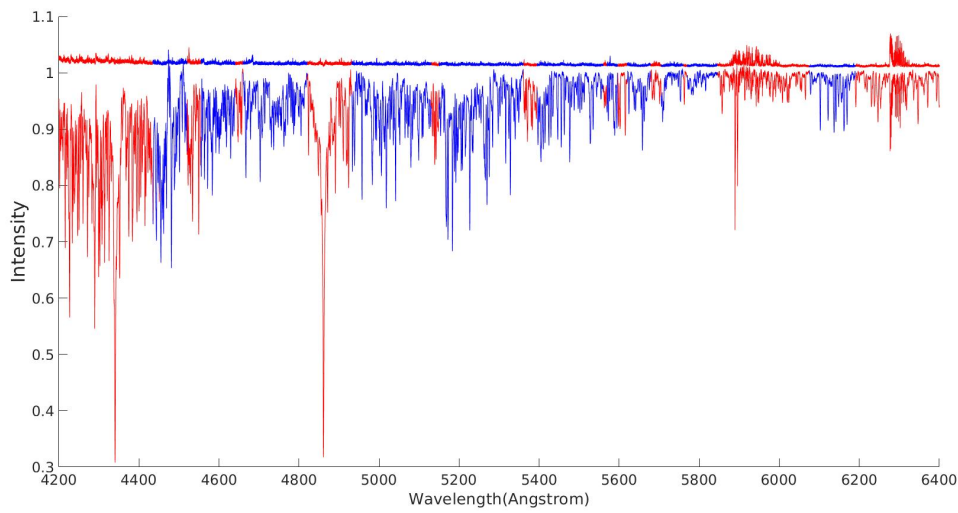


Figure 8: The mean spectrum from HD 139095, with hydrogen, telluric and unusable regions removed, the red sections are the ones that were removed, the blue sections are saved. The top line shows the standard deviation from the mean spectra, regions with large values need to be removed.

A cross-correlation technique is used to improve the signal-to-noise ratio of the line profile from that of each line individually. This is done by cross-correlating the spectrum with that of the mean spectrum. This produces a profile that can be used to determine frequencies present in the original spectrum. The accuracy of this function is greatly improved with a series of δ -functions positioned at each spectral line. Once cross-correlated, a profile is obtained that represents all the lines with delta functions in a template. The template is generated corresponding to the wavelength positions and intensities of each of the accepted lines from a synthetic spectrum. These δ -functions are scaled to the depths of the lines that they represent using a least squares fit. This is done to provide a cross-correlation function that is weighted in favour of stronger lines. It is assumed that all the individual lines have equal pulsation phase. To make this assumption more accurate lines with equivalent widths less than 5.0 \AA are removed. It is also important to note that it is assumed all the δ -functions are varying in a similar way. This isn't the case, however, because spectral lines can behave differently due to temperature and gravity variations caused by non-radial pulsations [37]. The δ -function template is cross-correlated with the spectral lines which are then interpolated onto the same radial velocity axis. This method is repeated for each observation to create a cross-correlated representative line profile.

4.5 FAMIAS

FAMIAS is the acronym for Frequency Analysis and Mode Identification for Asteroseismology Software. It was used to complete the Fourier analysis on the prepared time-series spectra in order to obtain the frequencies and modes [41]. It utilises two techniques using photometric and spectroscopic data. FAMIAS is specifically designed to perform the seismic modelling. It is applicable to main-sequence pulsators hotter than the Sun, this includes γ -Doradus stars. A pixel-by-pixel method is utilised in FAMIAS, this is a line-profile variation method that looks at the moment of each pixel in the spectral absorption line, they are then analysed as a time series via a calculation of a Fourier spectrum. A Fourier spectrum of the frequencies present in the line profile is then created for each pixel. An average is taken for each pixel to get the Fourier spectrum that shows the mean amplitude across the line for a range of frequencies. An alternative method for identifying frequencies is the moment method. This method finds frequencies in the various moments of the line profile (the equivalent width, radial velocity, variance and skewness moments). The pixel-by-pixel method and moment method both offer accurate techniques for identifying frequencies. It was suggested in a comparative test in 2004 that the pixel-by-pixel method offers a more constrained value of azimuthal order [42]. This method will therefore be used for this project.

The selection process for accepting frequencies is defined by: greater signal-to-noise ratio than 4 (frequencies with $\text{SNR} \leq 4$ are considered not significant), and below the Nyquist frequency. The Nyquist frequency is the higher limit for which a periodic frequency can be found. For regularly sampled data the Nyquist frequency is $1/2\delta t$ where δt is the average sampling rate [43]. This boundary is introduced to limit the occurrence of harmonics which are multiples of a known frequency. If the frequencies satisfy the conditions they are accepted into the least-squares fitting, in order of decreasing amplitude.

The data are then fitted with non-linear multi-periodic least-squares fit of a sum of sinusoids. The fitting is applied to every bin of the spectrum separately, the fitting formula is as follows:

$$Z + \sum_i A_i \sin[2\pi(F_i t + \phi_i)], \quad (9)$$

Z is the zero-point, A_i , F_i and ϕ_i are amplitude, frequency and phase (in units of 2π), respectively, of the i -th frequency. This equation is used to determine the zero-point, amplitude and phase profile for each frequency (ZAP profile).

The time series is then pre-whitened, a process that makes the data behave statistically like white noise. This reduces the dynamic range of the strongest signal by flattening the spectrum, the signal can then be approximated by a δ -function. The process can then be repeated for the next strongest frequency until there are no longer any more significant frequencies to extract. The signal-to-noise ratio for each frequency is calculated from the noise from the Fourier spectrum of pre-whitened data.

The determined ZAP profiles need to be manually inspected. Identifying which ZAP profiles are interdependent of each other requires some experimentation of different frequency selections. The standard deviation and phase fits of frequencies that appear unaffected for all different permutations, are frequencies that can be considered intrinsic to the star. Harmonics are integer multiples of intrinsic frequencies and so it is important to identify these and remove them. If adding a frequency causes another to disappear then one of those frequencies is likely to be an alias. Alias frequencies are the sum of an integer number of days and a known frequency, these are identified and removed. Combinations of multiple frequencies also occur and again need to be rejected. The amount of anomalous frequencies that can appear can make finding the intrinsic frequencies time consuming as care needs to be taken

not to accept them into the mode identification.

The mode identification technique is applied to the least-squares fit of the selected frequencies. A Fourier parameter fit method is used in FAMIAS, which uses the rotational broadening of the line profile, it has been determined to be superior for mode identification of stars that have $v \sin i > 30 \text{ km s}^{-1}$ [2]. The least-squared fits were imported to the mode identification tab and the selected frequencies and dispersion bins determine the zero-point values, amplitude and phase. The method is reliant upon the fact each pixel across the line profile varies in intensity with the same period for each pulsation mode.

The following initial stellar parameters need to be set: effective temperature of the stellar surface; $\log g$, the value of the logarithm of gravity at the stellar surface; the metallicity [Fe/H] and the central wavelength, these values are given in table 4.

Star	Effective Temp (K)	$\log g$	[Fe/H]	Reference
HD 139095	7093	3.51	0.071	[23]
HD 48501	7240	4.28	0.15	[44]
HD 197541	6977	3.89	-0.11	[45]

Table 4: The literature values for the atmospheric stellar parameters that were used in FAMIAS.

A zero-point fit is computed using these coefficients, this Gaussian fit of the line-profile determines the $v \sin i$; the equivalent width of the-line profile; intrinsic width of the line profile, unbroadened by stellar rotation and zero-point line-profile velocity offset. This step can be computed multiple times each iteration reducing the parameters individual range until a fixed value can be determined. Once these values are fixed, the mode identification can commence. This introduces further free parameters that need to be fixed: radius, mass, inclination and importantly, the degree and azimuthal order of the pulsation mode. This is the step that is the most costly in terms of computational time, and a balance must be found between speed and accuracy of the fit.

4.6 Error Calculations

A derivation of the errors for least-squares fitting to time-series data is as follows. Using a time-series signal to determine frequency presents errors originating from uneven sampling of data in time; the noise superimposed on the sinusoidal signal may be correlated in time as well as being non-Gaussian and aliasing of the initial signal. The one-sigma error in frequency, $\sigma(f)$, due to noise in the observed magnitudes with a root-mean-square (RMS) deviation of $\sigma(m)$ is given by

$$\sigma(f) = \sqrt{\frac{6}{N}} \frac{1}{\pi T} \frac{\sigma(m)}{a}, \quad (10)$$

where N is the total number of data points, T is the total base line of observations and a is the amplitude of the frequency, f . The relation between $\sigma(m)$ and the one-sigma error in amplitude, $\sigma(a)$, (a value that is calculated within FAMIAS) can be used to determine $\sigma(f)$ with respect to $\sigma(a)$ [46] as

$$\sigma(a) = \sqrt{\frac{2}{N}} \sigma(m), \quad (11)$$

$$\sigma(f) = \frac{\sqrt{3} \sigma(a)}{\pi T a}. \quad (12)$$

The relationship in equation (12) will be used to determine the errors in the least-squares fitting of each frequency. It is important to note that this error derivation was done using the assumption of uncorrelated noise and therefore is the lower bound of potential realistic errors. Equation (12) also stresses the importance of a large time baseline of observations, T , as this is inversely proportional to the error size.

The Fourier parameter fit method calculated the chi-square (X^2) value which is regarded as the goodness of the fit. Combining complex amplitude and phase information from theoretical and observational ZAP profiles a value for X^2 can be calculated as

$$X^2 = \frac{1}{2n_\lambda} \sum_{i=1}^{n_\lambda} \left[\frac{(A_{R,i}^o - A_{R,i}^t)^2}{\sigma_{R,i}^2} + \frac{(A_{I,i}^o - A_{I,i}^t)^2}{\sigma_{I,i}^2} \right], \quad (13)$$

where n_λ is the number of pixels across the profile, σ is the observational error, N is the number of free parameters, A^o is the observational amplitude defined by A_R and A_I as the real and imaginary components of the complex amplitude and A^t is the theoretical amplitude defined by the same complex components [41]. Using this value for chi-square the standard deviation, s^2 in the measurement can be defined as

$$s^2 = X^2 \frac{\sigma^2}{(n-1)}, \quad (14)$$

n being the sample size. The relationship between standard deviation and standard error is:

$$SE = \frac{s}{\sqrt{n}}, \quad (15)$$

where SE is the standard error. Combining equations (14) and (15) the expression for SE can be determined with respect to X_v^2 in equation (16),

$$SE = \sqrt{\frac{\sigma^2 X^2}{n(n-1)}}. \quad (16)$$

The large sample size makes the assumption $n(n-1) = n^2$ and so the final expression for the SE is:

$$SE = \frac{\sqrt{\sigma^2 X^2}}{n}. \quad (17)$$

None of the potential systematic errors have been accounted for during this error derivation because it is based on a perfect spectral series. Identifying the exact line position is complicated by broadening and blending of the lines, this is mainly caused by the effect of the star's rotation. It is extremely difficult to accurately model how much of an affect the rotation has on the errors because the inclination of the star is unknown. Research is currently being done on Rossby-modes (r -modes) and modelling them might be able to indicate the stellar inclination [21]. An r -mode pulsation is caused by a star's rotation and so they propagate in the same direction, modelling them would directly reveal the inclination of the star. More research needs to be completed on r -modes to make this a possibility in the future.

The results will be detailed in separate sections for each target star with an individual discussion at the end of the section. The cross-correlation functions from which the frequencies are extracted are shown and the mean Fourier spectrums for each of the selected frequencies are given. The Fourier parameter fit results are detailed before the final mode identification results. An example of the amplitude and phase profiles for a selected mode are shown with an explanation of the fit.

5 HD 139095 Results

5.1 Cross-Correlation function

The cross-correlation profiles for HD 139095 are shown in figure 9. It is possible to estimate the radial velocity offset with respect to Earth by using the minimum of the profile, this value appears to be -5 km s^{-1} but will be confirmed during the Fourier parameter fit. A variation in the line profile can clearly be seen, this represents the pulsating behaviour.

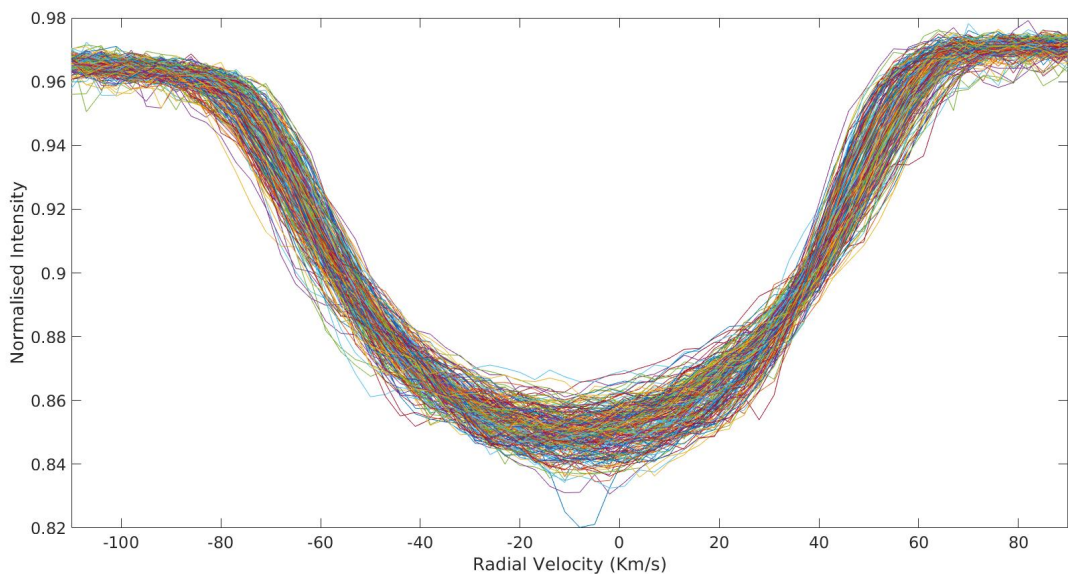


Figure 9: HD 139095 cross correlation profiles showing the variation in the line profile. Each colour represents a separate observation, 257 in total.

5.2 Frequency Identification

From the cross-correlation function five significant frequencies have been identified all of which exceed the minimum $SNR \geq 4$ limit, table 5. All of the periods shown are similar to those of a γ -Dor. All the frequencies display similar amplitudes suggesting there is not one dominant pulsation mode. Figure 10 shows the mean Fourier spectrum from which the frequencies were extracted. Once the frequency with the highest amplitude (f_1) was removed through pre-whitening, the frequency with the next highest amplitude was identified. This process was repeated until no more significant frequencies were identified.

This is apparent when comparing the first mean Fourier spectrum and the last one, f_5 is clearly less prominent. This method is susceptible to selecting aliases, harmonics and combinations. These need to be removed during inspection of the least-squares fit. Table 6 shows the frequencies that were detected as a result of aliasing. The frequency f_5 is identified as a two-day alias of f_4 , f_6 can be described as a combination of f_1 and f_3 and f_7 appears to be the result of the third harmonic of f_4 . An extra frequency was identified as $2.29234 \pm 0.00003\text{d}^{-1}$ It appeared to be intrinsic as it was unaffected during experimentation with the least-squares fits however with a SNR of only 3.378 it was removed because the signal was not strong enough to perform an accurate mode identification. In future projects with more spectra this frequency may be identified again. The larger amount of spectra may result in it passing the SNR limit of ≥ 4 .

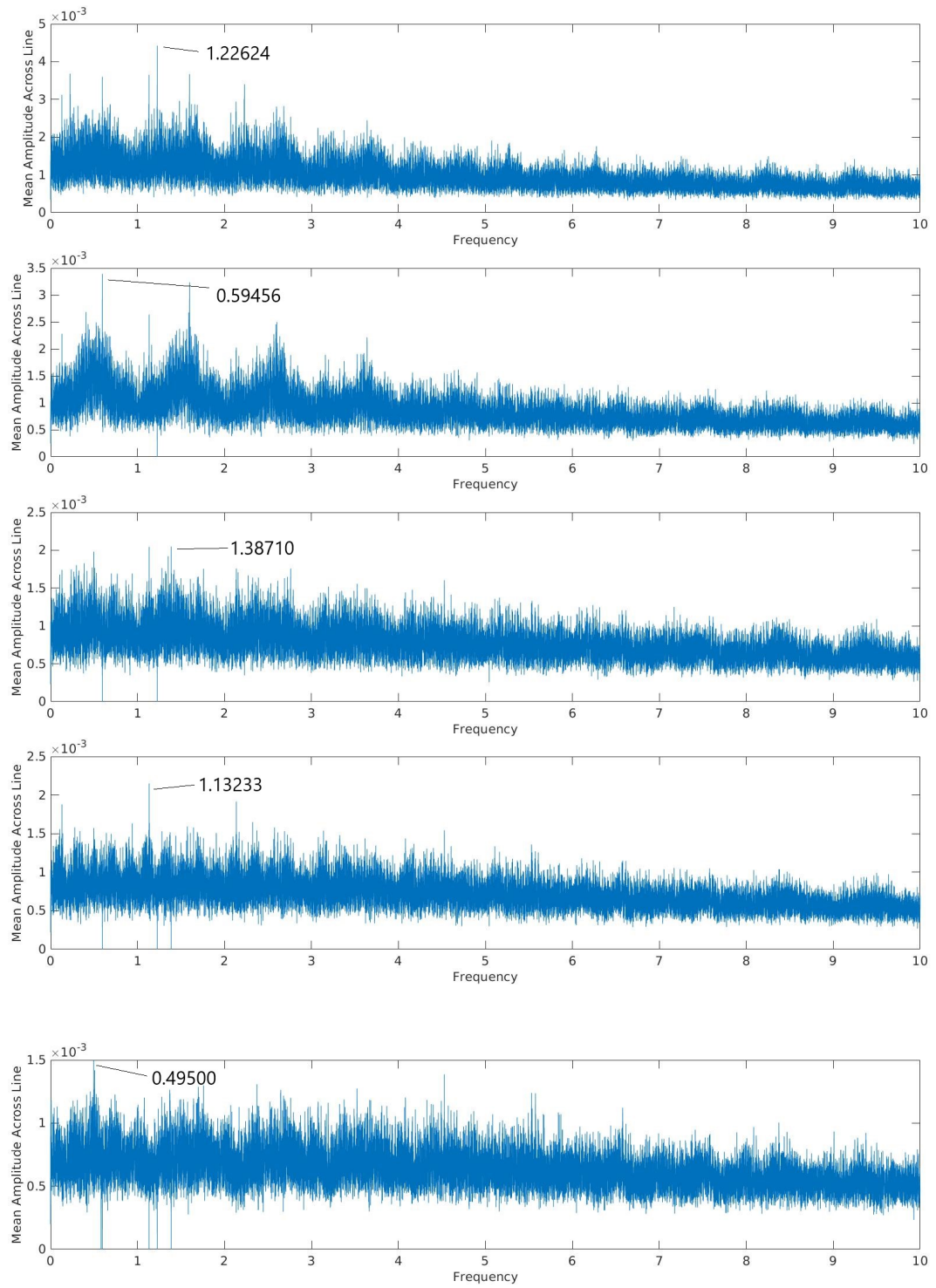


Figure 10: HD 139095, the pixel-by-pixel mean Fourier spectrum showing the intrinsic frequencies stated in table 5. All the frequencies have units of d^{-1} . The top Fourier spectrum is that of the full spectra where f_1 was identified. After being accepted into the least-squares fitting, the data is pre-whitened leading to second Fourier spectrum. This process is repeated until all intrinsic frequencies are extracted.

	$f1$	$f2$	$f3$	$f4$	$f5$
Frequency (d^{-1})	1.22624 ± 0.00001	0.59456 ± 0.00002	1.38710 ± 0.00002	1.13233 ± 0.00001	0.49500 ± 0.00002
Period (d)	0.81550 ± 0.00005	1.68192 ± 0.00003	0.72093 ± 0.00009	0.88313 ± 0.00007	2.02022 ± 0.00006
Amplitude	0.632 ± 0.018	0.530 ± 0.024	0.333 ± 0.22	0.475 ± 0.017	0.328 ± 0.017
SNR	14.106	9.822	7.669	14.198	6.447

Table 5: The frequency, period, amplitude and SNR values for the five significant pulsation frequencies from HD 139095.

	$f5$	$f7$	$f8$
Frequency (d^{-1})	3.38565 ± 0.00009	2.67845 ± 0.00006	3.389486 ± 0.000003
Alias combination	$f4 + 2$	$f1+f4$	$f4 \times 3$

Table 6: A list of removed frequencies that were created as a result of aliasing for HD 139095.

5.3 Fourier Parameter Fit and Mode Identification

The parameters for the mode identification are derived from the literature values in table 4. The parameters $\nu \sin i$, inclination, equivalent width, intrinsic width, mass, radius and velocity offset were initially set as free. Once the chi-square value in the fit had been reduced significantly, these values could then be constrained. The values with the best fit are shown in table 7 below.

Chi-square	$M(M_{\odot})$	$R(R_{\odot})$	Inclination ($^{\circ}$)	$\nu \sin i$ (kms^{-1})	Equivalent Width (kms^{-1})	Intrinsic Width (kms^{-1})	Velocity Offset (kms^{-1})
32.3457	2.867 ± 0.006	2.601 ± 0.009	5.9 ± 0.05	68.7 ± 0.1	19.73 ± 0.05	17.32 ± 0.04	-4.31 ± 0.01

Table 7: The determined stellar parameters for HD 139095.

A $\nu \sin i$ value of $68.7 \pm 0.1 kms^{-1}$ is suggested, this is similar to the $\nu \sin i$ indicated in the literature of 65.3^{-1} . The $\nu \sin i$ parameter remained constant whilst the other zero-point parameters were allowed to vary when a grid search was performed to identify the modes. The atmospheric parameters only weakly affect the fit and so constraining $[M/H]$, T_{eff} and $\log g$ is not a significant constraint. a radial velocity offset of $-4.31 \pm 0.01 kms^{-1}$ is given and confirms the estimate from the cross-correlation profile.

The mode identification results are displayed in table 8 for the frequencies $f1$, $f2$, $f3$ and $f4$. The suggested mode identification indicates modes of (1,1), (2,-1), (3,0) and (2,-2), respectively. The phase and amplitude values indicate the frequencies are independent and all intrinsic to the star. The amplitude and phase plot for $f3$ are shown in figure 11 as an example. This frequency has modes of (3,0) to a chi-square value of 3.48737. The fit (displayed by the line) for the phase plot appears to be the reflection of the actual phase (the data points), this can happen because $\pm\pi$ is equal to the same phase. The plots for frequencies $f1$, $f2$ and $f4$ are included in the appendix.

Frequency	Chi-square	$R(R_{\odot})$	$M(M_{\odot})$	Inclination ($^{\circ}$)	l	m	Velocity Amplitude	Phase (2π rad)
f_1	10.5508	3.9333 ± 0.0002	1.2667 ± 0.0001	47.25 ± 0.02	1	1	1.2903 ± 0.0001	0.2047 ± 0.0002
f_2	11.0585	1.5333 ± 0.0001	1.8321 ± 0.0001	39.351 ± 0.005	2	-2	1.9355 ± 0.0003	0.1575 ± 0.0004
f_3	3.48737	4.4667 ± 0.0001	1.3454 ± 0.0002	49.354 ± 0.003	3	0	5.8065 ± 0.0001	0.9448 ± 0.0002
f_4	12.7354	3.6667 ± 0.0002	3.4012 ± 0.0001	42.347 ± 0.001	2	-2	3.8710 ± 0.0002	0.4567 ± 0.0003

Table 8: The results of the mode identification for HD 139095.

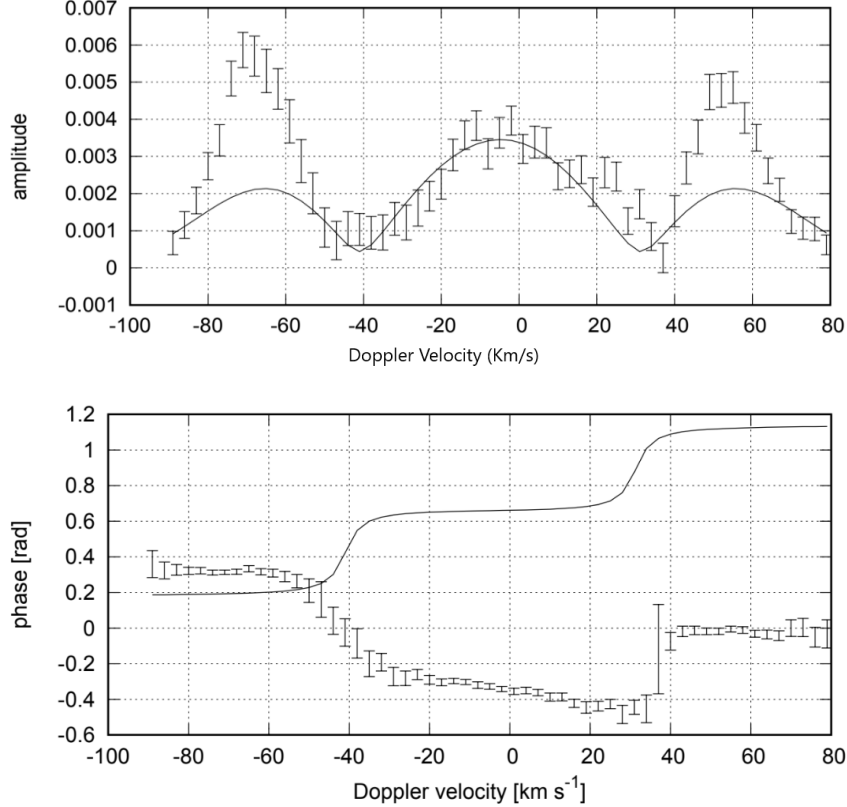


Figure 11: The amplitude and phase profiles for f_3 , showing pulsation mode of (3,0). The line shows the fit, the data points are observation with an error confined by the limits. The phase fits are cyclic and the phase is given in 2π radians

5.4 Discussion HD 139095

The frequencies identified for HD 139095 are $f_1 = 1.22624 \pm 0.00001 \text{ d}^{-1}$, $f_2 = 0.59456 \pm 0.00002 \text{ d}^{-1}$, $f_3 = 1.38710 \pm 0.00002 \text{ d}^{-1}$, $f_4 = 1.13233 \pm 0.00001 \text{ d}^{-1}$ and $f_5 = 0.49500 \pm 0.00002 \text{ d}^{-1}$. f_1 , f_3 and f_4 are closely spaced but there is no indication that they are related. Previous photometric research identified HD 139095 to have one period of 0.634 days, equivalent to 1.585 d^{-1} . This does not relate directly to the intrinsic frequencies found in this project however there is an alias combination of f_2 that matches, $f_2 + 1 \rightarrow 1.595 \text{ d}^{-1}$. Aliasing is a common problem with identifying frequencies in γ -Dors, which means confusion may arise during frequency identifications. This highlights the need for more spectroscopic analysis of γ -Dor stars. The photometric identification of HD 139095 done previously failed to identify the multiple pulsation frequencies uncovered in this project and may have incorrectly identified another

period that isn't intrinsic to the star because of the limited number of observations. Further spectroscopic identification needs to be completed to definitively determine the nature of the frequency at 1.585 d^{-1} .

The Phase and amplitude fits shown in Figure 11 and those in the appendix suffer from large distortions. This indicates there are still several more modes yet to be identified. When these frequencies beat in phase together they have the ability to create very large distortions and an inaccuracy in the line profile. This impedes the fit. In particular the frequency $f3$ could be affected by the closely spaced frequencies $f4$ and $f5$. Further analysis into these frequencies would be needed to confirm this discrepancy. The errors given should only be taken as a minimum because none of the potential systematic errors are accounted for. The effect of the rotation on the line profile is also not well defined due to the inclination being a variable that is calculated as part of the modelling.

As expected with the spectroscopic results analysed in 2008 [30], it is difficult to compare any of the frequencies with these results. Possible combinations of the intrinsic frequencies found in the results were explored and an explanation for $f1$ (2.353 d^{-1}) in the 2008 experiment was found. It seems to be a combination of the frequencies $f1 + f4$ from these observations, correct to 3 significant figures. However the other frequencies haven't been identified to be the result of multiple combinations, aliases and harmonics as they don't satisfy the standard period limit (periods ≥ 0.3 days) of g -mode pulsations. These frequencies should still be searched for in future studies because although they may not be the result of g -modes they could reveal another pulsation mechanism with a shorter period. These higher frequencies could be an indication of the p -modes that can be found in δ -Scuti stars, a class that HD 139095 was initially a part of when first defined [27]. More spectroscopic or photometric data needs to be obtained to definitively define the origin of the frequencies identified in the 2008 experiment and potentially re-classify HD 139095 as a δ -Scuti- γ -Doradus hybrid. The TESS mission that observes this star in sectors five and six in short cadence mode (2 min) will provide these data.

An interesting aspect of this star is its relatively-high rotation rate. Confirmed in this project as $68.7 \pm 0.1 \text{ kms}^{-1}$, it will make an excellent candidate in the work to categorise Rossby-modes. These modes will be easier to identify thanks to the high rotation rate. Using the determined modes of the star in this project along with future work with Rossby-modes the effects of rotation on the internal stellar structure can be analysed.

The mode identification of HD 139095 categorised $f1$ as a sectorial mode of (1,1), $f2$ a retrograde (2,-2), $f3$ a prograde (3,0) and $f4$ another retrograde (2,-2). A prograde mode has an azimuthal order of $m \leq 0$, retrograde has $m \geq 0$ and a sectorial mode identifies as $m = \pm l$ [47]. There have been no published previous full mode identifications of HD 139095 and so these results are extremely valuable going forward with the aim to fully model all known γ -Doradus stars..

6 HD 197541 Results

6.1 Cross-correlation function

The cross-correlation function of HD 197541 appears unusually narrow for a γ -Doradus star as seen in figure 12. This indicates a low $v \sin i$. An estimation of the velocity offset is approximately 20 kms^{-1} , the Fourier parameter fit will confirm this value. There appears to be distinct variation in the line-profile. This variation is particularly visible on the wings of the profile, a characteristic of strong pulsating behaviour.

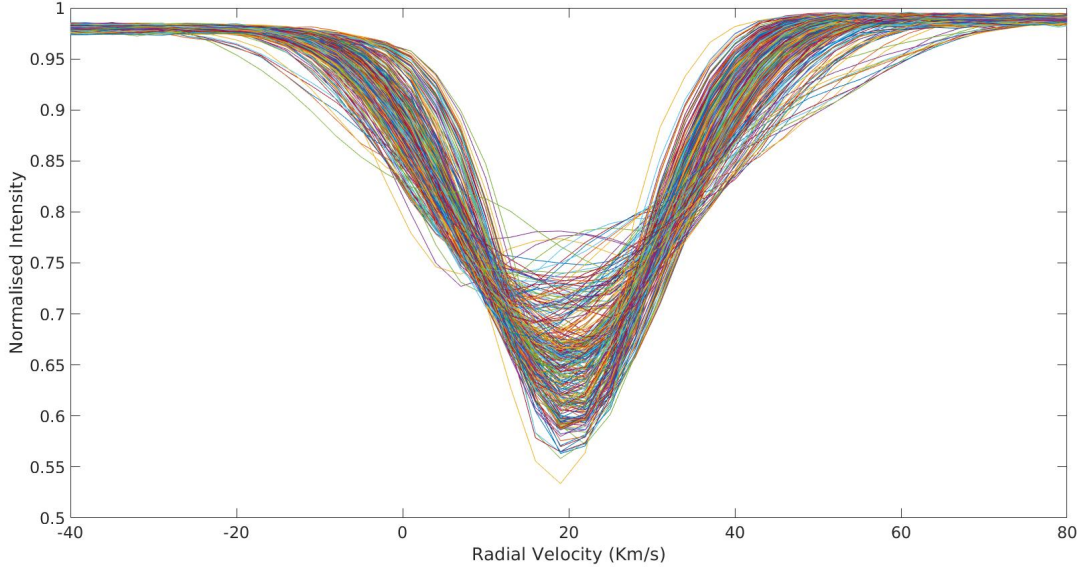


Figure 12: HD 197541 cross-correlation profiles showing the variation in the line-profile. The total of 309 spectra is displayed by different coloured lines.

6.2 Frequency Identification

The six significant frequencies that were identified during the pixel-by-pixel mean Fourier spectrum are shown in table 9. An exception to the $SNR \geq 4$ was allowed for frequency f_4 because experimentation of the ZAP profiles from the least-squares fitting indicates it as intrinsic to the star. This frequency also has a relatively large amplitude in comparison to the other frequencies which is another factor in the decision to carry it forward for mode identification. The frequency $f_2 \approx 1$ indicating it has the possibility to be a one day alias, however the amplitude profile indicates it to be intrinsic. Figure 13 shows the pixel-by-pixel mean Fourier spectrum for HD 197541. The frequency with the highest amplitude is shown by the top Fourier spectrum, it is quite clear to identify the first three frequencies by inspection. After the data had been pre-whitened multiple times it is harder to distinguish the following significant frequencies. This is because they are more hidden by the noise of the spectra. Extra care is needed during the manual inspection of the least-squares fitting to ensure all the aliases, combinations and harmonics are removed. The aliases with a significant SNR that were rejected are stated in table 10. f_7 is the second harmonic of f_3 it had a SNR of 4.467 and passes the limit for acceptance there, highlighting the importance for this manual check. f_8 is a combination of f_3 and f_4 , interestingly f_9 is the resultant second harmonic of f_8 .

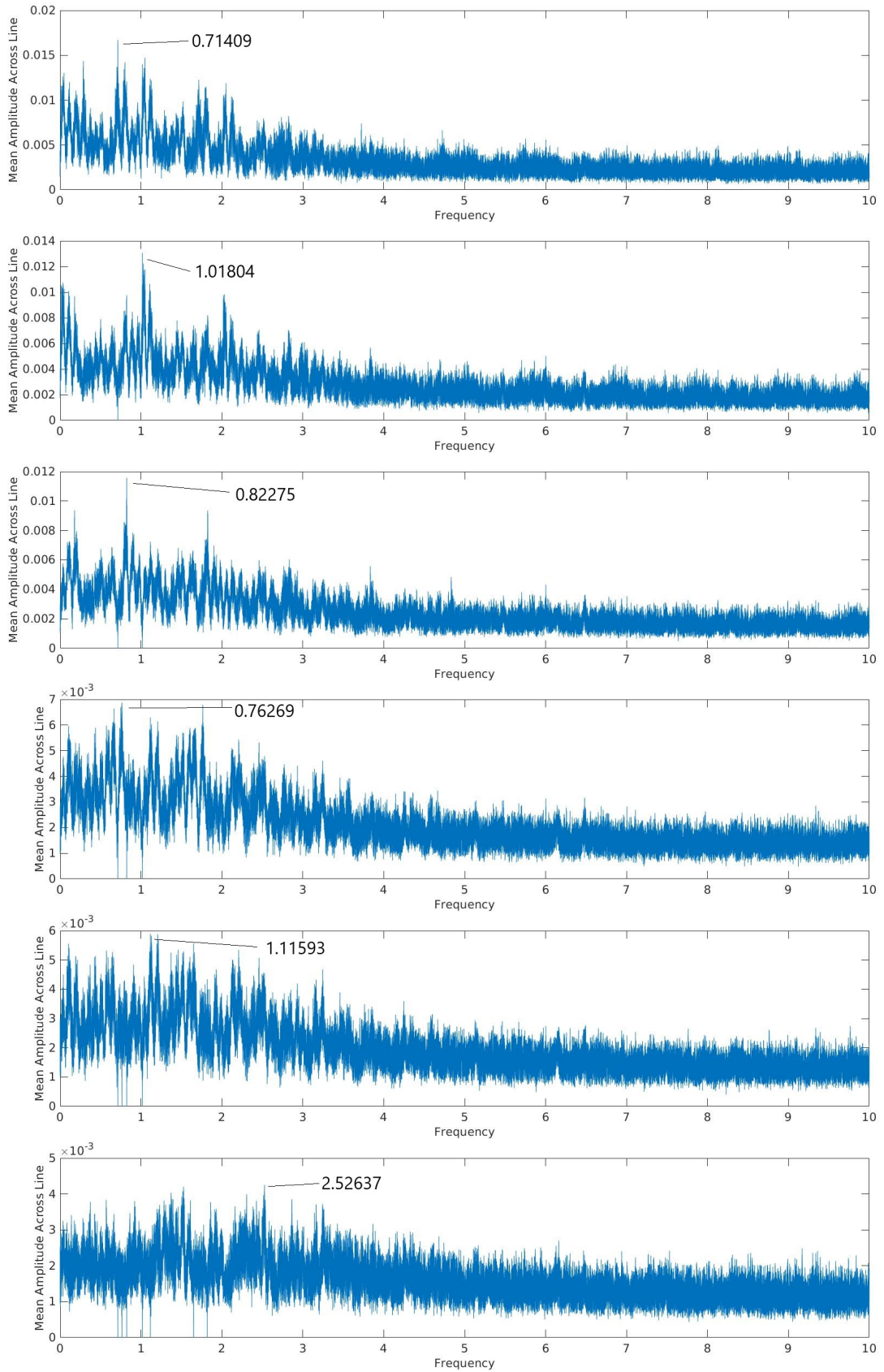


Figure 13: HD 197541, the pixel-by-pixel mean Fourier spectrum showing the frequency all the intrinsic frequencies stated in table. All the frequencies are given with values of d^{-1} . The most significant frequencies by amplitude start at the top and decrease down as the data is pre-whitened

	$f1$	$f2$	$f3$	$f4$	$f5$	$f6$
Frequency (d^{-1})	0.71409 ± 0.00001	1.01804 ± 0.00002	0.82275 ± 0.000007	0.76269 ± 0.00002	1.11593 ± 0.00002	2.52637 ± 0.00003
Period (d)	1.40038 ± 0.00003	0.98228 ± 0.00002	1.21544 ± 0.00007	1.31115 ± 0.00006	0.89611 ± 0.00004	0.39582 ± 0.00005
Amplitude	1.117 ± 0.08	1.235 ± 0.12	1.179 ± 0.05	0.616 ± 0.09	0.561 ± 0.04	0.367 ± 0.07
SNR	6.294	6.878	9.482	3.749	5.979	4.507

Table 9: The six most significant frequencies determined for HD 197541

	$f7$	$f8$	$f9$
Frequency (d^{-1})	1.651 ± 0.0001	1.589 ± 0.00007	3.166 ± 0.0003
Alias combination	$f3 \times 2$	$f1+f4$	$f8 \times 2$

Table 10: A list of removed frequencies that were created as a result of aliasing for HD 197541.

6.3 Fourier Parameter Fit and Mode Identification

Using the literature parameters given in table 4 the mass, radius, inclination, $v \sin i$, equivalent width, intrinsic width and velocity offset were calculated to a best-fit shown in table 11. The chi-square value of the fit is 31.4334. The $v \sin i$ is lower than expected when compared to the literature value (29 kms^{-1}) in table 2. It was left as a free parameter for the mode analysis for this reason. This low $v \sin i$ if proven correct would provide an explanation for the narrow cross-correlation profile 12. The radial velocity offset value of $33.62 \pm 0.06 \text{ kms}^{-1}$ is slightly higher than the estimation made using the cross-correlation function.

Chi-square	$M(M_{\odot})$	$R(R_{\odot})$	Inclination ($^{\circ}$)	$v \sin i$ (kms^{-1})	Equivalent Width (kms^{-1})	Intrinsic Width (kms^{-1})	Velocity Offset (kms^{-1})
31.4334	1.952 ± 0.006	2.597 ± 0.009	69.4 ± 0.2	7.5 ± 0.3	10.10 ± 0.05	8.95 ± 0.03	33.62 ± 0.06

Table 11: The result of the Fourier parameter fit for HD 197541.

The equivalent width, intrinsic width and velocity offset were set as fixed parameters for the mode identification. The modes for five frequencies, $f1$, $f2$, $f3$, $f4$ and $f6$ were determined as (3,-2), (2,-2), (3,-3), (3,-2) and (3,-1), respectively (table 12). The $v \sin i$ during this identification increased for each frequency and represents a value more comparable to that found in the literature table 2. It is still smaller marginally than the literature value however affirming it to be a possible reason for the narrow line-profile seen in figure 12. Phase and amplitude values suggest these frequencies are independent and intrinsic to the star. $f5$ could not have an accurate mode identification performed as the chi-square value indicated that a representative fit could not be found, despite adjustments to the stellar parameters. It proved difficult to achieve a lower chi-square value of the fits for $f1$, $f2$ and $f3$ even with the experimentation of the stellar parameter constraints. $f4$ and $f6$ display much lower chi-square values and give a better mode identification for those frequencies.

Frequency	Chi-square	$R(R_{\odot})$	$M(M_{\odot})$	Inclination ($^{\circ}$)	$v \sin i$ (kms^{-1})	l	m	Velocity Amplitude	Phase (2π rad)
$f1$	30.7257	2.0323 ± 0.0008	0.5807 ± 0.0005	63.65 ± 0.05	20.39 ± 0.02	3	-2	5.1613 ± 0.0001	0.5669 ± 0.0001
$f2$	16.7264	2.5967 ± 0.0003	0.5806 ± 0.0005	50.95 ± 0.03	24.89 ± 0.03	2	-2	3.8710 ± 0.0001	0.3701 ± 0.0002
$f3$	24.3274	0.8226 ± 0.0002	1.1452 ± 0.0002	66.19 ± 0.02	24.11 ± 0.01	3	-3	9.0322 ± 0.0001	0.0630 ± 0.0003
$f4$	6.42881	2.1129 ± 0.0004	1.1456 ± 0.0003	31.27 ± 0.04	20.59 ± 0.02	3	-2	0.6452 ± 0.0001	0.8268 ± 0.0002
$f6$	4.35642	2.7581 ± 0.0002	1.2258 ± 0.0004	64.286 ± 0.002	22.64 ± 0.01	3	-1	10.968 ± 0.001	0.7008 ± 0.002

Table 12: Table of the full mode identification of HD 197541.

The amplitude and phase plots for frequency $f4$ are shown in figure 14 as an example of the fit, with a chi-square value of 6.42881. This frequency can be stated to have a pulsation mode (3,-2). The phase

fit line looks extremely accurate because of the small error bars and accurate fitting. The rest of the fits for the frequencies f_1 , f_2 , f_3 and f_6 for HD 197541 are given in the appendix.

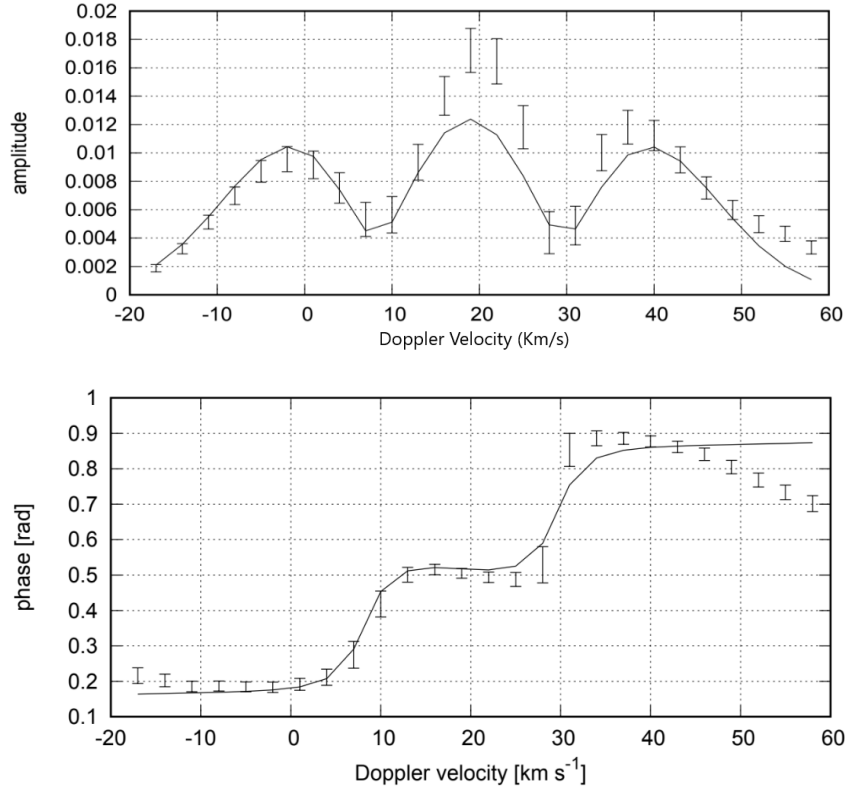


Figure 14: The amplitude and phase profiles for f_4 , showing pulsation mode of (3,-2). The line shows the fit, the data points are observation with an error confined by the limits. The phase fits are cyclic and the phase is given in 2π radians

6.4 Discussion HD 197541

Six frequencies for HD 197541 were identified as $f_1 = 0.71409 \pm 0.00001 \text{ d}^{-1}$, $f_2 = 1.01804 \pm 0.00002 \text{ d}^{-1}$, $f_3 = 0.82275 \pm 0.000007 \text{ d}^{-1}$, $f_4 = 0.76269 \pm 0.00002 \text{ d}^{-1}$, $f_5 = 1.11593 \pm 0.00002 \text{ d}^{-1}$ and $f_6 = 2.52637 \pm 0.00003 \text{ d}^{-1}$. The period of 1.4 days (0.71 d^{-1}) discovered in 1999 from HIPPARCOS photometry is confirmed in this project corresponding to the frequency, f_1 ($0.71409 \approx 0.71429$). In regards to the period of 1.093, this doesn't represent any of frequencies determined by the pixel-by-pixel mean Fourier spectrum. This could be because it fell below the $\text{SNR} \geq 4$ criteria and therefore wasn't detected during this project. A future project with a larger set of spectra may be able to identify this frequency. There appears to be a large range of pulsating frequencies determined by the identification. This suggests a thorough frequency analysis. Even though an thorough analysis is indicated, there is still some distortion in the phase and amplitude fits that could be explained by other resonating frequencies impeding the fit. The TESS photometric data obtained in sector one in short cadence mode may reveal more frequencies.

This project determined that the $v \sin i$ of 29 km s^{-1} shown in the literature is high. The Fourier parameter fit obtained a value of $7.5 \pm 0.3 \text{ km s}^{-1}$ and, although this value increased during the mode identification, the results suggest that the accepted value should be reduced. A smaller $v \sin i$ would also provide an explanation for the narrow line profile seen in the cross-correlation function. Stars with low rotation rates suffer from less line broadening.

There has been no previous mode identification published and so the determined modes in this project are extremely valuable. The mode determined for; f_1 , f_2 , f_3 , f_4 and f_6 were all retrograde (3,-2), (2,-2), (3,-3), (3,-2) and (3,-1) respectively.

7 HD 48501 Results

7.1 Cross-correlation function

The cross-correlation function for HD 48501 is made up of observations from both the 1-port and 4-port files (figure 15). The original plan was to create cross-correlation functions for both 1-port and 4-port individually however there is not enough observations separately to produce a representative function. Alternatively the frequency and mode identification will be computed using a mix of the two. It will be possible to draw the conclusions about the 4-port observations from comparing the mixed results with literature values. It is a positive sign that the cross-correlation profile has no outlying lines, indicating the reduction of the 4-port observations was successful. The radial velocity offset for HD 48501 appears to be large at about 45 km s^{-1} , this value will be confirmed during the parameter fit. There is a lot of variability that can be seen around the minimum of the function. This is representative of a lot of pulsating behaviour.

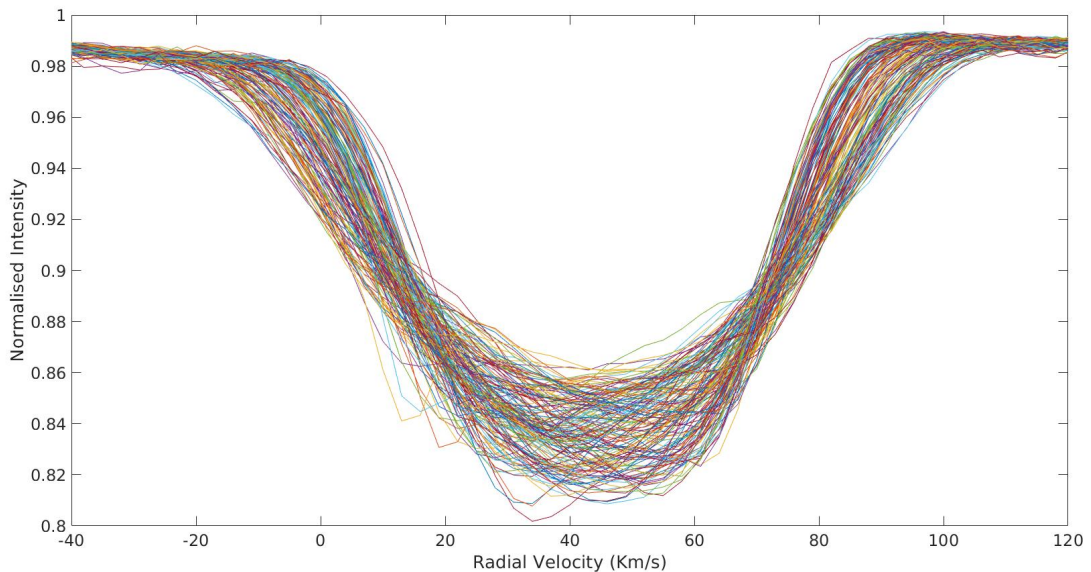


Figure 15: HD 48501 cross correlation profiles. Each colour represents a separate observation, 165 in total.

7.2 Frequency Identification

Four significant frequencies were extracted from the cross-correlation function, they are displayed in table 13. The pixel-by-pixel mean Fourier spectrum shows the position of the four selected frequencies,

figure 16. One frequency, f_1 appears to be the dominant frequency, displaying a SNR of $3\times$ that of the other frequencies. f_4 has a similar pulsation period to that of the dominant f_1 and so its pulsation mode may be difficult accurately determine due to merging. In general, the pulsation periods of the four frequencies are similar of around one day, this could make the mode determination difficult especially with f_1 being so dominant. The Fourier spectra show very clearly the frequencies f_1 and f_2 . Once they are removed during the pre-whitening, it is more difficult to identify the following frequencies because of their lower amplitude. As expected, the dominant f_1 had an alias frequency detected as f_5 which is its second harmonic. Another harmonic is identified as f_6 which is the second harmonic of f_3 shown in table 14.

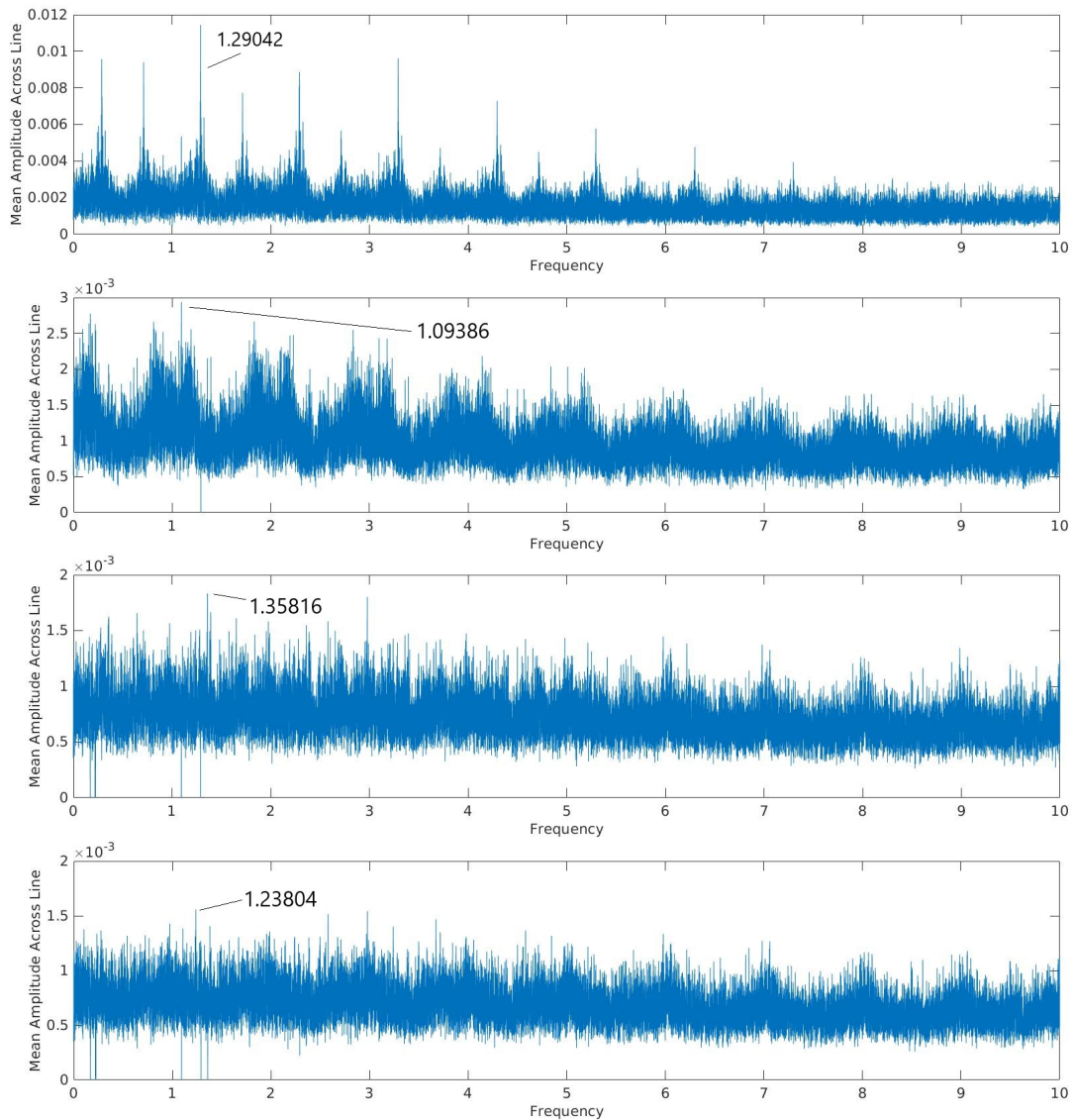


Figure 16: HD 48501, the pixel-by-pixel mean Fourier spectrum showing the frequency all the intrinsic frequencies stated in table 13. All the frequencies are given with units of d^{-1} . The frequency with the largest amplitude is at the top and can clearly be identified. the amplitudes decrease rapidly as the significant frequencies are removed.

	$f1$	$f2$	$f3$	$f4$
Frequency (d^{-1})	1.29042 ± 0.00003	1.09386 ± 0.00005	1.35816 ± 0.0002	1.23804 ± 0.0002
Period (d)	0.77494 ± 0.00006	0.91419 ± 0.00003	0.73629 ± 0.00004	0.80773 ± 0.00005
Amplitude	1.439 ± 0.12	0.466 ± 0.08	0.309 ± 0.2	0.209 ± 0.14
SNR	14.904	4.851	4.424	4.183

Table 13: The four significant frequencies from the cross-correlation profile for HD 48501.

	$f5$	$f6$
Frequency (d^{-1})	2.58069 ± 0.00003	2.70974 ± 0.00005
Alias combination	$f1 \times 2$	$f3 \times 2$

Table 14: A list of removed frequencies that were created as a result of aliasing for HD 48501.

7.3 Fourier Parameter Fit and Mode Identification

The Fourier parameter fit to the zero-point profile is shown in table 15. This displays a velocity offset of $41.4 \pm 0.04 \text{ kms}^{-1}$, which is similar to that from the estimate using the cross-correlation profile. The $v \sin i$ is calculated in this fit is higher than the literature quoted value of 29 kms^{-1} from table 2 and so will be set as a free parameter during the mode identification.

Chi-square	$M(M_{\odot})$	$R(R_{\odot})$	Inclination ($^{\circ}$)	$v \sin i$ (kms^{-1})	Equivalent Width (kms^{-1})	Intrinsic Width (kms^{-1})	Velocity Offset (kms^{-1})
27.1612	2.597 ± 0.006	2.274 ± 0.003	8.38 ± 0.002	44.1 ± 0.1	10.33 ± 0.03	12.67 ± 0.04	41.4 ± 0.04

Table 15: The result of the Fourier parameter fit for HD 48501.

The results of the mode identification fitting to the frequencies $f1$, $f2$, $f3$ and $f4$ give modes of (2,-2), (2,-2), (2,-2) and (3,-3) respectively given in table 16. The lowest chi-square value for $f1$, displayed in the table, is relatively large in comparison to the other frequencies. Comparing the phase and amplitude of the frequencies, it's apparent that the pulsations are independent and intrinsic to the star. The $v \sin i$ computed during these fits appears to be a lot more representative because it is much slower, it is also similar to the value given in the literature. An example of the (2,-2) pulsation can be seen in figure 17. The amplitude and phase profile were taken from the dominant frequency $f1$. A quadruple peak is fitted to the amplitude profile, this is to include the slight centre double peak in the data. This double peak is hard to discern and could possibly be just a singular peak as would be seen in mode (1,-1). A decision was made to categorise this frequency as (2,-2) but more analysis needs to be done with more spectra to definitively define the frequencies mode. The rest of the profiles are given in the appendix for frequencies $f2$, $f3$ and $f4$.

Frequency	Chi-square	$R(R_{\odot})$	$M(M_{\odot})$	Inclination ($^{\circ}$)	$v \sin i$ (kms^{-1})	l	m	Velocity Amplitude	Phase (2π rad)
$f1$	23.6714	2.516 ± 0.005	1.548 ± 0.002	29.38 ± 0.005	35.7 ± 0.1	2	-2	2.0459 ± 0.0001	0.9606 ± 0.0003
$f2$	2.61168	2.6774 ± 0.003	2.0320 ± 0.003	15.10 ± 0.01	32.5 ± 0.2	2	-2	1.8065 ± 0.0002	0.410 ± 0.004
$f3$	1.87385	2.7581 ± 0.0008	1.7097 ± 0.0009	19.03 ± 0.005	39.8 ± 0.2	2	-2	1.9355 ± 0.0001	0.2677 ± 0.0002
$f4$	0.91541	2.6774 ± 0.0003	1.7098 ± 0.0002	3.78 ± 0.02	31.2 ± 0.1	3	-3	6.4516 ± 0.0002	0.7952 ± 0.0001

Table 16: The full mode identification values for HD 48501.

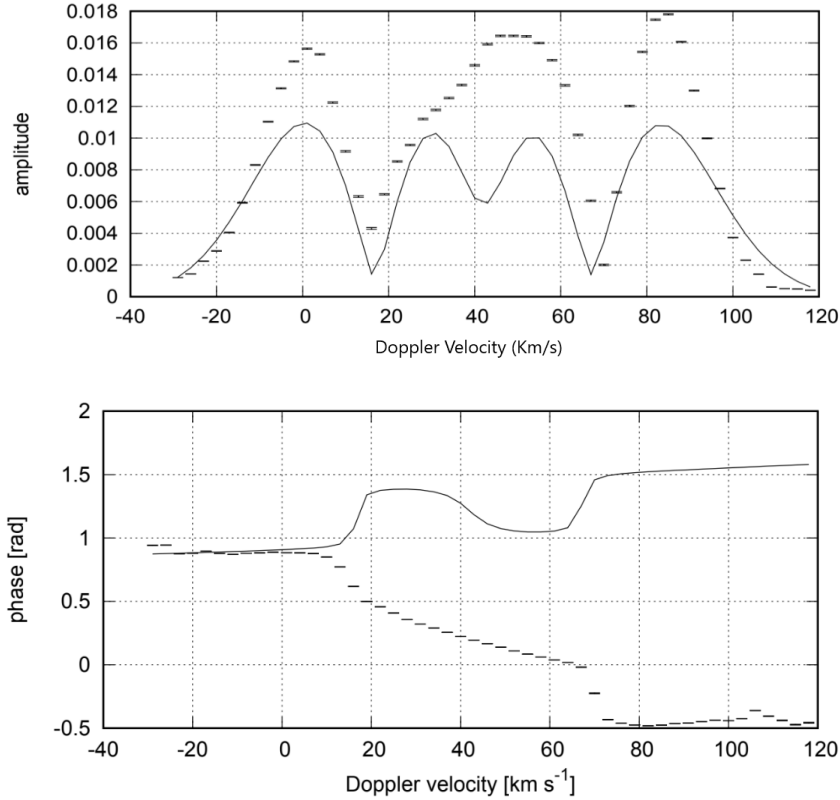


Figure 17: The amplitude and phase profiles for f_1 , showing pulsation mode of (2,-2). The line shows the fit, the data points are observation with an error confined by the limits. The phase fits are cyclic and the phase is given in 2π radians

7.4 Discussion HD 48501

The pixel-by-pixel mean Fourier spectrum revealed four frequencies $f_1 = 1.29042 \pm 0.00003 \text{ d}^{-1}$, $1.09386 \pm 0.00005 \text{ d}^{-1}$, $1.35816 \pm 0.0002 \text{ d}^{-1}$ and $1.23804 \pm 0.0002 \text{ d}^{-1}$. Thanks to significant work being done on HD 48501 in the past there is a the possibility to compare the sets of results. Of the three frequencies identified by Aerts et al 2004, two of them directly correspond to f_1 and f_2 in this project, see table 18. This confirms the validity of the results. Two extra frequencies were also obtained showing the value of completing this analysis. There was, however, one frequency identified by Aerts that this spectroscopic observation didn't determine, $f_5 = 1.19924 \text{ d}^{-1}$. A more extensive observation with a longer time-baseline may uncover this frequency and more. The TESS mission will provide this extra data during its sixth and seventh sector observations in short cadence mode.

	f_1	f_2	f_3	f_4	f_5
Results (d^{-1})	1.29042	1.09386	1.35816	1.23804	
Literature (d^{-1})	1.29054	1.09408			1.19924

Table 17: Comparison of the HD 48501 frequencies from results and literature [33].

The spectroscopic analysis done in 2004 categorised all modes as $l=1$. The modes for f_1 , f_2 , f_3 and f_4 were determined to be (2,-2), (2,-2), (2,-2), (3,-3). The limited amount of observations, only

34 spectra, could be the reason for the difference in the two results. The 165 spectra used in this project demonstrates the importance of obtaining as much data as possible when completing a mode identification. As the literature frequency 1.19924 d^{-1} was not detected in this project no comment can be made of the $l=1$ classification stated. The value of 29 kms^{-1} from the 2004 project was also confirmed in this project. This value having been determined by two separate experiments over 15 years apart means that it can be considered as definitive.

8 Sources of error

As stated previously, the errors calculated using the equation 17 are purely statistical based on perfect spectra. It should be stated that the low uncertainty determined due to the long time base of the observations means that these errors should be treated as minimum values. The reality is that these error values underestimate the true error and are used as a guide. There are a number of non-statistical sources of error that give an indication of the true scale of the error value. The $v \sin i$ causes an uncertainty caused by rotational effects. If the effects of the Coriolis force are significant, it can cause a distortion on the stellar surface. For this reason there needs to be a solution formulated to quantify this error in future work.

The technique used when formulating the modes for each frequency gives the best result where the chi-square (X^2) value is at a minimum. The X^2 quantifies how good the fit is where X^2 should approximately equal the number of degrees of freedom to be considered a good fit. An accurate fit should be described as having a X^2 value of less than 30. The only fit that exceeded this value was $f1$ of HD 197541. This X^2 value would be reduced if more spectra was obtained, something to consider in the next analysis of this star.

9 Further discussion and conclusions

This project was extremely successful in its aims. All three target stars had a full frequency and mode identification performed upon them, shown in table 19. Fourier analysis was used to extract four significant frequencies from HD 48501, five for HD 139095 and six for HD 197541. Manual inspection was used to remove any other frequencies that appeared significant but were alias, harmonic or combination frequencies. The results from this project were compared to those of previous experiments. A particular important conclusion from this was the discovery of the origin of $f1$ from the 2008 photometric experiment of HD 139095. It was determined to be a combination of the two intrinsic frequencies $f1$ and $f4$ from this project. Confirming the values for HD 48501 and HD 139095 was extremely important. Having been stated in the errors, the rotational effects are often the limiting factor in deriving an accurate error value and hence confirming the $v \sin i$ is extremely useful for future projects. The $v \sin i$ of HD 197541 is suggested to be re-evaluated as a slower value than the 29 kms^{-1} found in the literature. The results of this experiment indicate a value of around 20 kms^{-1} but extra research needs to be completed on this.

Star	Frequency (d^{-1})	(l,m)	Phase(2π rad)
HD 139095	$f1 = 1.22624$	(1,1)	0.2047
	$f2 = 0.59456$	(2,-2)	0.1575
	$f3 = 1.38710$	(3,0)	0.9448
	$f4 = 1.13233$	(2,-2)	0.4567
HD 197541	$f1 = 0.71409$	(3,-2)	0.5669
	$f2 = 1.01804$	(2,-2)	0.3701
	$f3 = 0.82275$	(3,-3)	0.0630
	$f4 = 0.76269$	(3,-2)	0.8268
	$f5 = 2.52637$	(3,-1)	0.7008
HD 48501	$f1 = 1.29042$	(2,-2)	0.9606
	$f2 = 1.09386$	(2,-2)	0.4095
	$f3 = 1.35816$	(2,-2)	0.2677
	$f4 = 1.23804$	(3,-3)	0.7952

Table 18: A table summarising the results of the full frequency and mode identification for the three target stars.

All the target stars display frequencies typical of γ -Doradus stars. The star HD 189631 is a bona fide γ -Doradus star with extensive frequency and mode analysis already completed in 2018. Four frequencies of $f = 1.6774 \pm 0.0002 d^{-1}$, $f2 = 1.4174 \pm 0.0002 d^{-1}$, $f3 = 0.0714 \pm 0.0002 d^{-1}$ and $f4 = 1.8228 \pm 0.0002 d^{-1}$ with modes of (1,1), (1,1), (2,-2) and (1,1) respectively [48]. This was a multi-site high-resolution spectroscopic study with a total of 479 spectra obtained. The large amount of spectra means this project is regarded as extremely accurate. With the exception of $f3$ all the frequencies are of a similar value to the ones found in the target γ -Dors. The errors found in both sets of results are of the same magnitude, this is because the same statistical approach was used. The modes determined in the 2018 project are again very similar to the ones from these results. Of the total thirteen modes, seven of those are (1,1) and (2,-2) modes, concluding that these are the most prevalent pulsating modes in γ -Doradus stars. A conclusion that was also noticed in the 2018 project.

Comparing the results of all the stars, all the frequencies are in the same range. There are no particular outlying frequencies with the largest, HD 197541's $f5$, and the smallest, HD 139095's $f2$, only a value of $1.93181 d^{-1}$ less. The standard guide line for the frequency limits of γ -Doradus stars is $0.33 d^{-1} \leq f_x \leq 3.33 d^{-1}$. All of the determined frequencies fall within these limits. The most frequencies and modes identified were for HD 197541, this is expected because had the most spectra obtained, 309. HD 139095 had five identified frequencies and four of those were fit for mode identification due to its 257 spectra. HD 48501 had the least spectra and had four frequencies identified with them all used in the mode identification. This follows the trend that the more spectra obtained the more frequencies and modes can be identified, stressing the importance of gaining a large amount of data. The separation of the four frequencies of HD 48501 is small, this could be another affect of the limited spectra. A larger data set could unveil a more differential range of frequencies. The smaller amount of data available for HD 48501 highlights the importance of using the 4-port data alongside the 1-port. The results look consistent with the other γ -Dors in the experiment and with the previous work done on this star. It is therefore concluded that the 4-port files are equally as accurate as the 1-port. Any future analysis that needs to be conducted on the 4-port spectra should utilise this method for its reduction.

Conclusions can be made with regards to the difference in $v \sin i$ of HD 139095 and the other stars. HD 139095 had a determined $v \sin i$ of $68.7 \pm 0.1 \text{ kms}^{-1}$. This is higher than that of the other rotation rates and may be reflected in the difference in determined modes. Stars HD 197541 and HD 48501 have consistent pulsating modes throughout their frequencies, of HD 48501's four modes, three are (2,-2). The modes for HD 197541 are all retrograde with four of the five frequencies' spherical degree, equal to three. In contrast of the four modes of HD 139095, there is a sectorial (1,1) mode, two retrograde (2,-2) modes and a prograde (3,0). This lack of consistency could be due to the effects of the faster rotation

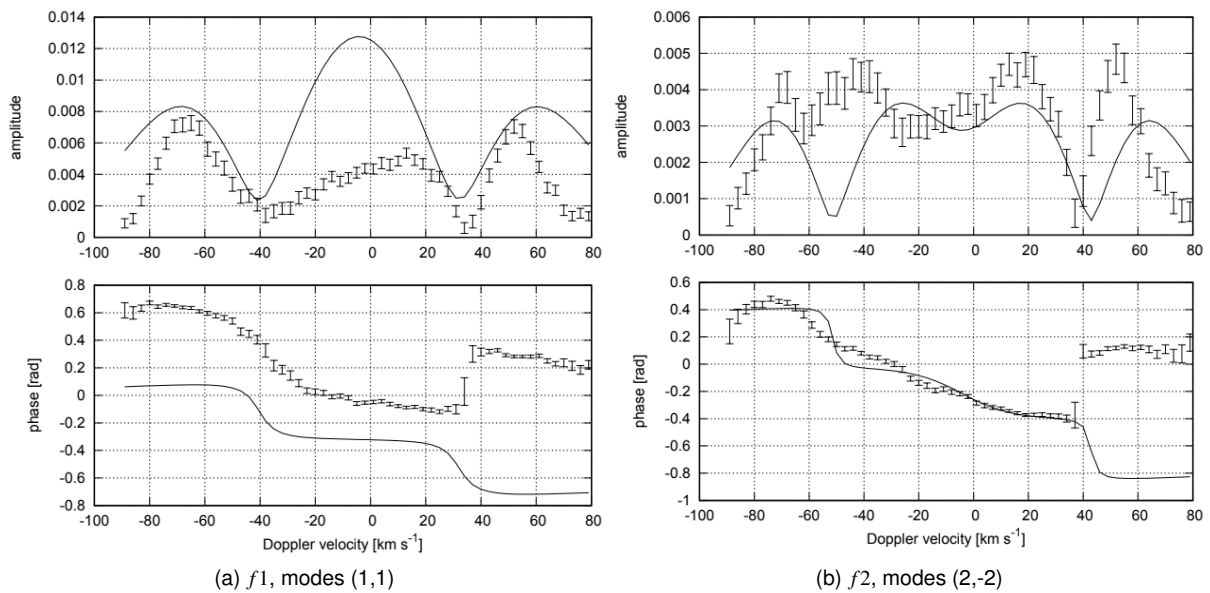
rate. It is known that the rotation rate of γ -Doradus stars can affect their pulsations, but the severity of this is not well understood. It could be possible that a faster rotation rate results in a more dispersed set of modes. More research into the effects of rotation on the stellar interior needs to be completed.

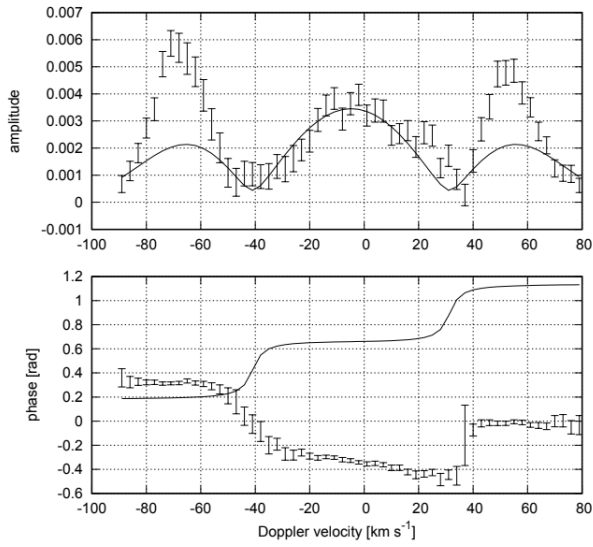
In future work on these target stars, more data would perhaps identify frequencies that this project missed. With that aimed this data could be used alongside the TESS photometric mission of which all three stars are observed by. An interesting aspect of future work would be to explore the rotational properties of HD 139095 further with respect to Rossby-modes. This star is a prime candidate in that field because of its moderate-high $v\sin i$ producing Rossby- mode pulsations that will be observable. It has been proven in this experiment that accurate spectroscopic analysis of the stars g – modes can be completed irrespective of the rotation rate. This indicates that it has the perfect $v\sin i$ for this research.

In conclusion, this project not only contributes to the growing knowledge of the γ -Doradus class of pulsating star but should be utilised in any future work that involves these stars. All three target stars should be analysed further to be able to categorically state the known frequencies and modes. With this project's results an extra step is gained in the search to uncover the hidden information at the core of the γ -Doradus class of pulsating variables.

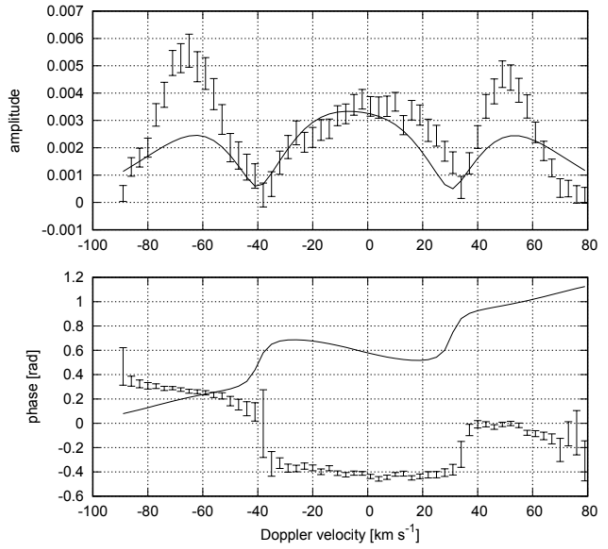
10 Appendix

10.1 HD 139095 phase and amplitude profiles





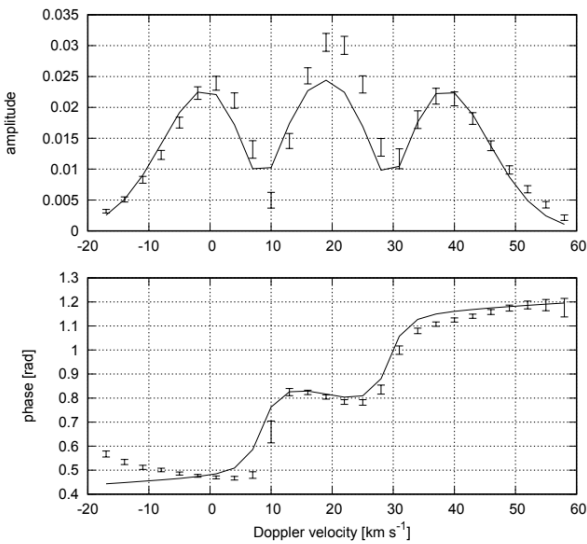
(c) f_3 , modes (3,0)



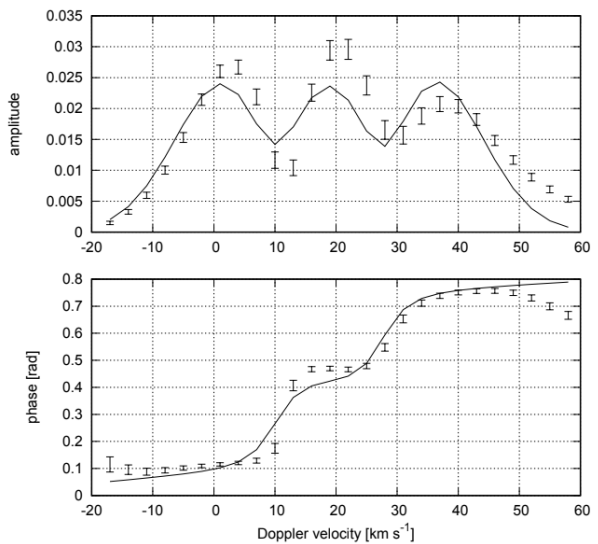
(d) f_4 , modes (2,-2)

Caption: The phase and amplitude profiles for HD 139095. The fit is represented by the solid line and the dots represent the data points with representative error bars. The phase fits are cyclic and the phase is given in 2π radians.

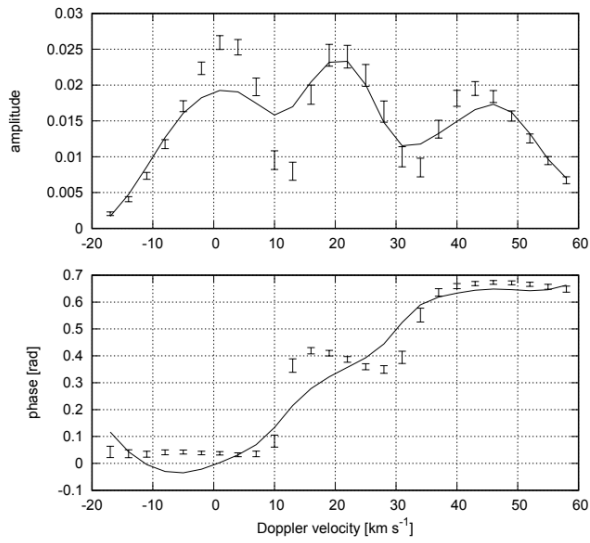
10.2 HD 197541 phase and amplitude profiles



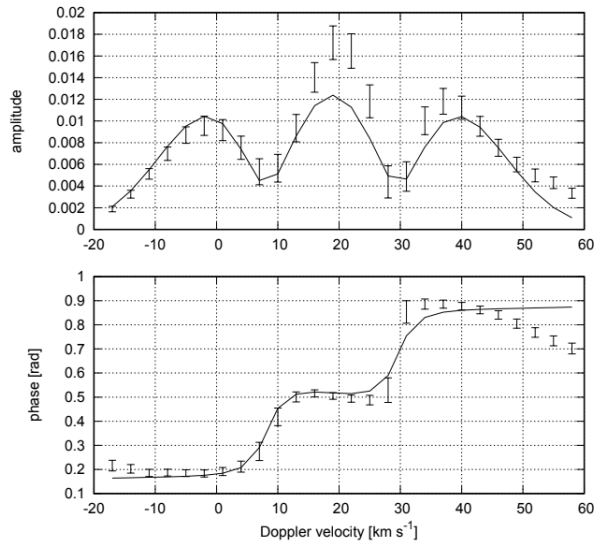
(e) f_1 , modes (3,-2)



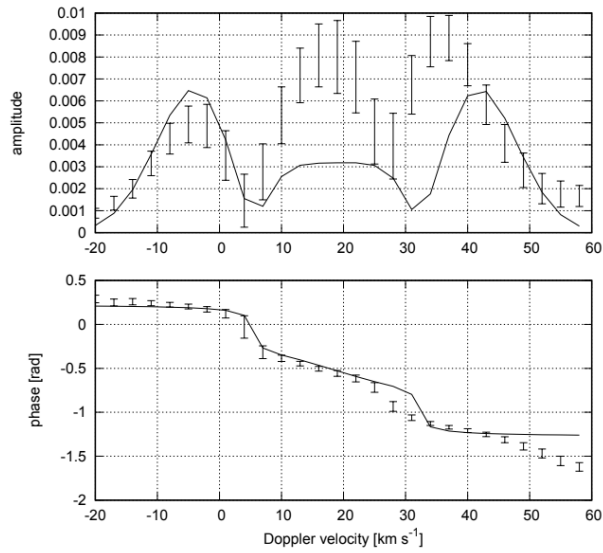
(f) f_2 , modes (2,-2)



(g) f_3 , modes (3,-3)



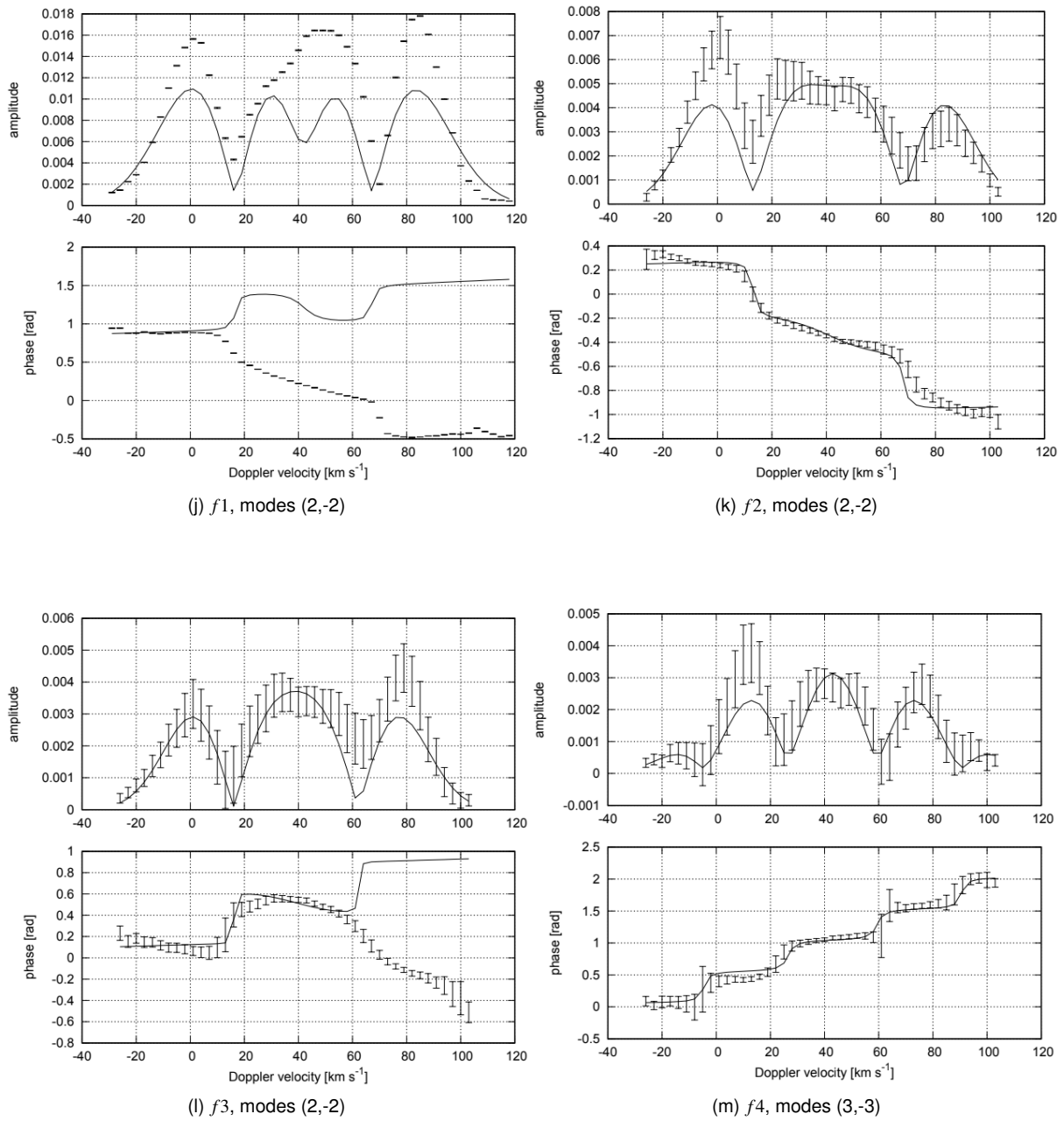
(h) f_4 , modes (3,-2)



(i) f_6 , modes (3,-1)

Caption: The phase and amplitude profiles for HD 197541. The fit is represented by the solid line and the dots represent the data points with representative error bars. The phase fits are cyclic and the phase is given in 2π radians.

10.3 HD 48501 phase and amplitude profiles



Caption: The phase and amplitude profiles for HD 48501. The fit is represented by the solid line and the dots represent the data points with representative error bars. The phase fits are cyclic and the phase is given in 2π radians.

References

- [1] Cassatella. A; Gura. D; Reimers. D; Stickland. D. Omicron Ceti. *Publications of the International Astronomical Union Circulars*, 1, Nov 1979.
- [2] Jayasinghe. T; Stanek. K. Z; Kochanek. C. S. The ASAS-SN catalogue of variable stars - II Uniform classification of 412 000 known variables. *Monthly notices of the Royal Astronomical Society*, 486:1907–1943, Jun 2019.
- [3] L. A. Balona; K. Krisciunas; W. J. Cousins. γ -Doradus: evidence for new class of pulsating star. *Monthly notices of the Royal Astronomical Society*, 270:905–913, 1994.
- [4] A. B. Kaye; G. Handler; K. Krisciunas. γ -Doradus Stars: Defining a New class of pulsating variable. *Publications of the astronomical society of the Pacific*, 111:840–844, July 1999.
- [5] E. Brunsden; K. R. Pollard; D. J. Wright; P. De Cat; P. L. Cottrell. Frequency and mode identification of γ -Doradus from photometric and spectroscopic observations. *Monthly notices of the Royal Astronomical Society*, pages 1–10, March 2018.
- [6] T. R. White; T. R. Bedding; D. Stello; J. Christensen-Dalsgaard; D. Huber; H. Kjeldsen. Calculating Asteroseismic Diagrams For Solar-Like Oscillations. *The Astrophysical Journal*, Oct 09.
- [7] H.J. Deeg. Five years of Exoplanet observations with the CoRoT space observatory. *European Planetary Science Congress*, 7:381, 2012.
- [8] W. J. Borucki; D. Koch; G. Basri; N. Batalha; T. Brown; D. Caldwell. Kepler Planet-Detection Mission: Introduction and First Results. *Science*, 327:977–980, Feb 2010.
- [9] T. L. Campante. The asteroseismic potential of TESS: exoplanet-host stars. *The Astrophysical Journal*, 830, Aug 2016.
- [10] K. Uytterhoeven; A. Moya; A. Grigahcène; J. A. Guzik; J. Gutiérrez-Soto; B. Smalley; G. Handler; L. A. Balona; E. Niemczura; L. Fox Machado; S. Benatti; E. Chapellier; A. Tkachenko; R. Szabó; J. C. Suárez; V. Ripepi; J. Pascual; P. Mathias; S. Martín-Ruiz; H. Lehmann; J. Jackiewicz; S. Hekker; M. Gruberbauer; R. A. García; X. Dumusque; D. Díaz-Fraile; P. Bradley; V. Antoci; M. Roth; B. Leroy; S. J. Murphy; P. De Cat; J. Cuypers; H. Kjeldsen; J. Christensen-Dalsgaard; M. Breger; A. Pigulski; L. L. Kiss; M. Still; S. E. Thompson; J. Van Cleve. The kepler characterization of the variability among A- and F-type stars. *Astronomy and Astrophysics*, 1:534, May 2011.
- [11] J. P. Sánchez Arias; A. H. Córscico; L. G. Althaus. Asteroseismology of hybrid δ -Scuti/ γ -Doradus pulsating stars. *Astronomy and Astrophysics*, 597, Dec 2017.
- [12] E. Brunsden; K. R. Pollard; P. L. Cottrell; D. J. Wright; P. De Cat. Spectroscopic pulsational frequency identification and mode determination of γ -Doradus star HD 12901. *Monthly notices of the Royal Astronomical Society*, pages 1–11, Nov 2018.
- [13] C. Aerts; J. Cuypers; M-A. Dupret; J. De Ridder; R. Scuflaire; L. Eyer. Photometric mode identification in the two γ -Doradus stars HD 12901 and HD 48501. *Institute of Astronomy*, Sep 2002.
- [14] G. Handler. Asteroseismology. *communications in Asteroseismology*, May 2012.
- [15] J. A. Guzik; A. B. Kaye; P. A. Bradley; A. N. Cox; C. Neuforge-Verheecke. A proposed pulsation driving mechanism for γ -Doradus variable stars. *ASP Conference series*, 259, 2002.
- [16] C. Antonio; T. Guillermo. The dependence of convective core overshooting on stellar mass: Reality check and additional evidence. *The Astrophysical Journal*, 876:134, May 2019.
- [17] L. Eyer; P. Dubath; S. Saesen; D. W. Evans; L. Wyrzykowski; S. Hodgkin; N. Mowlavi. From HIPPARCOS to Gaia. *New Horizons in Time-Domain Astronomy Proceedings IAU Symposium*, 285, 2011.

- [18] C. Aerts; L Eyer; E Kestens. The discovery of new γ -Doradus stars from the HIPPARCOS mission. *Astronomy and Astrophysics*, 337:790–796, Mar 1998.
- [19] Maisonneuve; F. Pollard; K. R. Cottrell; P. L. Wright; D. J. De Cat; P. Mantegazza; L. Kilmartin; P. M. Suárez; J. C. Rainer; M. Poretti. Frequency analysis and pulsational mode identification of two γ -Doradus stars: HD 40745 and HD 189631. *Monthly notices of the Royal Astronomical Society*, 415:2977–2992, Aug 2011.
- [20] S. A. Barnes. Gyrochronology and its usage for main sequence field star ages. *Proceedings IAU Symposium*, 285, 2008.
- [21] G. Li; T. Van Reeth; T. R. Bedding; S. J. Murphy; V. Antoci. Period spacings of γ -Doradus pulsators in the kepler field: Rossby and gravity modes in 82 stars. *Monthly notices of the Royal Astronomical Society*, pages 1–17, 2018.
- [22] Sinachopoulos. D; Gavras. P; Dionatos. O; Ducourant. C; Medupe. T. Ccd astrometry and components instrumental magnitude difference of 432 HIPPARCOS wide visual double stars. *Astronomy and Astrophysics*, 472:1055–1057, May 2007.
- [23] A. Greenwood. Spectroscopic analysis of γ -Doradus variable stars. *Thesis, University of Canterbury*, Feb 2014.
- [24] Handler. G. The domain of γ -Doradus variables in the Hertzsprung-Russell diagram. *Monthly notices of the Royal Astronomical Society*, 309:19–23, Oct 1999.
- [25] F. Royer; J. Zorec; A. E. Gómez. Rotational velocities of A-type stars. *Astronomy and Astrophysics*, 463:671–682, Jun 2007.
- [26] T. Barclay. TESS input catalogue updated. *Website found at: <https://heasarc.gsfc.nasa.gov/docs/tess/tess-input-catalog-updated.html> (accessed: 20/06/2019)*, 2019.
- [27] G. W. Henry; F. C. Fekel; S. M. Henry. Photometry and spectroscopy of 11 γ -Doradus stars. *The Astronomical Journal*, 113:1421–1440, Apr 2007.
- [28] G. Handler; R. R. Shobbrook. On the relationship between the δ -Scuti and γ -Doradus pulsators. *Monthly notices of the Royal Astronomical Society*, 333:251–261, Jun 2002.
- [29] F. Royer; J. Zorec; A. E. Gómez. Rotational velocities of A-type stars. III. velocity distributions. *Astronomy and Astrophysics*, 463:110, 2007.
- [30] Pollard. K. R; Wright. D. J; Zima. W; Cottrell. P. L; De Cat. High-resolution spectroscopy and mode identification in non-radially pulsating stars. *Communications in Asteroseismology*, 157:118–123, 2008.
- [31] L. Eyer; C. Aerts. A search for new γ -Doradus stars in the Geneva photometric database. *Astronomy and Astrophysics*, 200:3001, Nov 2000.
- [32] C. Aerts; J. Cuypers; P. De Cat. Long-term multicolour photometry and high-resolution spectroscopy of the two γ -Doradus stars HD 12901 and HD 48501. *Astronomy Astrophysics*, 415:1079–1088, 2004.
- [33] Aerts. C. Cuypers; J. De Cat P; Dupret. M. A. Long-term multicolour photometry and high resolution spectroscopy of the two γ -Doradus stars hd 12901 and hd 48501 astronomy. *Astronomy and Astrophysics*, 2004.
- [34] Karen R. Pollard; E. Brunsden; M. Davie; A. Greenwood; P L Cotrell. Spectroscopic mode identification of γ -Doradus stars: frequencies, modes, rotation and wave leakage. *Astronomy in focus*, 11:509–513, Aug 2015.
- [35] J. B. Hearnshaw; S. I. Barnes; N. Frost; G. M. Kershaw; G. Graham; G. R. Nankivell. HERCULES: A high-resolution spectrograph for small to medium-sized telescopes. *The Proceedings of the IAU 8th Asian-Pacific Regional Meeting*, 289, 2003.

- [36] G. Nave; C. J. Sansonetti; F. Kerber. Reference wavelengths of thorium and argon for the calibration of infrared astronomical spectrographs. *OSA Technical Digest Series*, 2007.
- [37] D. J. Wright. Spectroscopic mode identification in a sample of non-radially pulsating stars. *Thesis, University of Canterbury*, 2008.
- [38] J. T. Wright; J. D. Eastman. Barycentric corrections at 1 cm/s for precise Doppler velocities. *Publications from the The Astronomical Society of the Pacific*, Sept 2014.
- [39] Hubeny. I; Lanz. T. Synspec: General spectrum synthesis program. *Astrophysics Source Code Library*, Sep 2011.
- [40] N. Rudolf; H. M. Gunther; P. C. Schneider; J. H. M. M. Schmitt. Modelling telluric line spectra in the optical and infrared with an application to VLT/X-shooter spectra. *Astrophysics and Astronomy*, 113, Dec 2016.
- [41] Zima. W. FAMIAS user manual. *Communications in Asteroseismology*, 155:17–121, Oct 2008.
- [42] W. Zima; K. Kolenberg; M. Briquet; M. Breger. Moment method and Pixel-by-Pixel method: Complementary mode identification I. testing FG Vir-like pulsation modes. *Institute for Astronomy*, 144, 2004.
- [43] L. Eyer; P. Bartholdi. Variable stars: Which Nyquist frequency? *Astronomy and Astrophysics*, 135:1–3, Feb 1999.
- [44] Bruntt. H; De Cat. P; Aerts. C. A spectroscopic study of southern (candidate) γ -Doradus stars - II. Detailed abundance analysis and fundamental parameters. *Astronomy and Astrophysics*, 478:96–487, 2008.
- [45] Casagrande. L; Schoenrich. R; Asplund. M; Cassisi. S; Ramirez. I; Melendez. J; Bensby. T; Feltzing. S. Geneva-copenhagen survey re-analysis. *VizieR Online Data Catalog*, 353:47–50, 2011.
- [46] M. H. Montgomery; D. O'Donoghue. A derivation of the errors for the least squares fitting to time series data. *Publications from the Austrian Academy of Sciences*, July 1999.
- [47] M. A. Smith. Nonradial m-mode changes in the 53 persei variable orions. *The Astrophysical Journal*, 42:261–281, 1980.
- [48] M. W. Davie; K. R. Pollard; P. L. Cottrell; E. Brunsden; D. J. Wright; P. De Cat. Spectroscopic pulsational frequency and mode determination of the γ -Doradus star HD 189631. *Publications from the Astronomical Society of Australia*, 2018.